

Identifying the impact of local connectivity patterns on dynamics in excitatory-inhibitory networks

Yuxiu Shao*

*School of Systems Science, Beijing Normal University, Beijing, China
Laboratoire de Neurosciences Cognitives et Computationnelles, INSERM U960,
Ecole Normale Supérieure - PSL Research University, Paris, France*

David Dahmen

Institute for Advanced Simulation (IAS-6) Computational and Systems Neuroscience, Jülich Research Center, Jülich, Germany

Stefano Recanatesi

Technion, Israel Institute of Technology, Haifa, Israel

Eric Shea-Brown

*Department of Applied Mathematics and Computational Neuroscience Center, University of Washington, Seattle, WA, USA
Allen Institute for Brain Science, Seattle, WA, USA*

Srdjan Ostojic†

*Laboratoire de Neurosciences Cognitives et Computationnelles, INSERM U960,
Ecole Normale Supérieure - PSL Research University, Paris, France*

(Dated: November 28, 2024)

Networks of excitatory and inhibitory (EI) neurons form a canonical circuit in the brain. Seminal theoretical results on dynamics of such networks are based on the assumption that synaptic strengths depend on the type of neurons they connect, but are otherwise statistically independent. Recent synaptic physiology datasets however highlight the prominence of specific connectivity patterns that go well beyond what is expected from independent connections. While decades of influential research have demonstrated the strong role of the basic EI cell type structure, to which extent additional connectivity features influence dynamics remains to be fully determined. Here we examine the effects of pair-wise connectivity motifs on the linear dynamics in excitatory-inhibitory networks using an analytical framework that approximates the connectivity in terms of low-rank structures. This low-rank approximation is based on a mathematical derivation of the dominant eigenvalues of the connectivity matrix, and predicts the impact on responses to external inputs of connectivity motifs and their interactions with cell-type structure. Our results reveal that a particular pattern of connectivity, chain motifs, have a much stronger impact on dominant eigenmodes than other pair-wise motifs. In particular, an over-representation of chain motifs induces a strong positive eigenvalue in inhibition-dominated networks and generates a potential instability that requires revisiting the classical excitation-inhibition balance criteria. Examining effects of external inputs, we show that chain motifs can on their own induce paradoxical responses, where an increased input to inhibitory neurons leads to a decrease in their activity due to the recurrent feedback. These findings have direct implications for the interpretation of experiments in which responses to optogenetic perturbations are measured and used to infer the dynamical regime of cortical circuits.

INTRODUCTION

Circuits of excitatory and inhibitory (EI) neurons are believed to form the fundamental components of information-processing in the brain [1–4]. Network models of recurrently-connected excitatory and inhibitory units have therefore become an essential tool for understanding neural dynamics and computation. Such models have helped uncover fundamental principles such as the role of excitation-inhibition balance for sustaining irregular activity [5–9], and the importance of inhibition

for stabilizing neural activity [8, 10–12] and normalizing responses [13]. A phenomenon that has attracted particular attention are *paradoxical responses*, which refer to situations where an increase in the external input to the inhibitory neurons results in a decrease of their activity because of recurrent interactions [10–16]. Recent theoretical analyses have argued that such paradoxical responses to external inputs can reveal the dynamical regime of the underlying excitatory-inhibitory network [14, 17, 18], and these insights have been used to interpret experimental measurements of responses to optogenetic perturbations [19–21].

These seminal theoretical results on excitatory-inhibitory networks however are derived via a key simplifying assumption. In standard models, the strength of the synaptic coupling between any two neurons depends

* ivyerosion@gmail.com

† srdjan.ostojic@ens.fr

on their types, but is otherwise assumed to be an independent random variable uncorrelated across synapses. This assumption is typically used to reduce a full network to a simpler circuit model that describes how the mean activities of different populations interact through averaged synaptic weights (Fig 1(a,b)). Recent synaptic-resolution experimental datasets from various species and brain areas have however revealed the prevalence of non-trivial connectivity patterns [22–30]. In particular, a recently released dataset from mice and humans [23, 30] reported the prominence of second-order motifs - specific correlations between pairs of synapses, such as reciprocal, chain, convergent, and divergent motifs (Fig 1(c)) - that go well beyond what is expected from independent connections, and highlights the need for a theoretical understanding of the effects of such patterns. While the presence of reciprocal connectivity motifs has been long recognized and examined within network models [29], several studies have found their influence on recurrent dynamics to be relatively modest [30–33]. Other studies have argued for the importance of several types of synaptic motifs working together to determine statistical properties of network activity, such as average synchrony or correlation among neurons and network-wide dimensionality [30, 32, 34–40]. In a general theoretical analysis [35], chain motifs were found to have a dominant role in determining population-averaged responses of networks to their inputs. Nevertheless, the impact of chain motifs on excitation-inhibition balance – including central issues of stability and paradoxical responses – as well as the general interplay among these motifs and structures established by cell-type specific connectivity, remain open and intriguing questions.

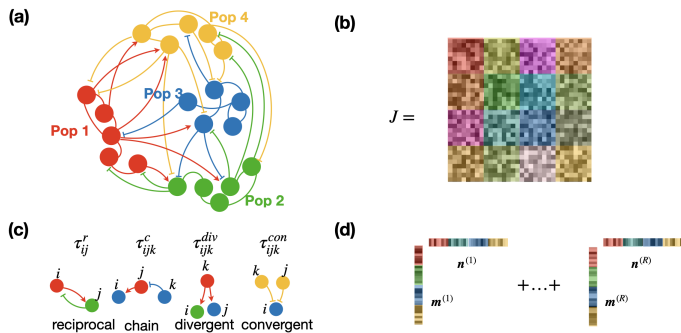


FIG. 1. Schematic of the multi-population network model. (a) The network consists of P populations, each represented by a different color. This population structure defines the statistics of synaptic connectivity. (b) The corresponding connectivity matrix consists of P^2 blocks. Synaptic weights within each block share identical statistical properties. (c) Four different types of second-order motifs, corresponding to different pair-wise correlations between synaptic weights. (d) A low-rank approximation of the connectivity matrix can integrate both the population structure and the pair-wise motif statistics.

In this study, we examine how the interaction between population structure and synaptic motifs influences re-

current dynamics and the presence of paradoxical responses. To this end, we expand a previously introduced theoretical framework that allows us to reduce large networks of multiple populations to a low-dimensional description that incorporates connectivity statistics beyond the mean via a low-rank approximation [33]. Applying this theory to excitatory-inhibitory networks with chain motifs, we demonstrate that these connectivity patterns significantly impact the eigen-spectrum of the connectivity matrix, and thereby the overall recurrent dynamics. Specifically, we found that chain motifs can create strong positive feedback even in inhibition-dominated networks, and are therefore a source of a potential instability that requires revisiting the classical conditions of excitation-inhibition balance. Moreover we show that chain motifs strongly influence the responses of different populations to external inputs, and can control whether the responses are paradoxical or not. These findings highlight the intricacy of the relationship between the responses to inputs and the underlying connectivity, and in particular sound a note of caution for interpreting results of experiments in terms of only average connectivity strengths among E and I cells.

This manuscript is organized as follows. **Sec. I** defines the connectivity and the network model. **Sec. II** introduces the general theoretical framework based on a low-rank approximation of the connectivity, which allows us to analytically investigate the effects of local motifs, in particular chain and reciprocal motifs, on recurrent dynamics and responses to external inputs. **Secs. III and IV** apply this theory to fully-connected and sparse excitatory-inhibitory networks with chain motifs. In **Sec. III** we analyze the influence of chain motifs on the eigenspectra of these models. In **Sec. IV**, we use these results to study the responses to external inputs and under what condition they are paradoxical.

I. NETWORK MODEL

A. Network connectivity

We consider networks of N recurrently connected neurons. The connectivity is represented by a matrix \mathbf{J} , where the entry J_{ij} corresponds to the synaptic weight from neuron j to neuron i . The statistics of network connectivity are then fully described by the joint distribution $\mathcal{P}(\{J_{ij}\})$ of the N^2 synaptic weights.

We assume that the network consists of P non-overlapping populations that determine the connectivity statistics as follows. The connectivity matrix \mathbf{J} has a $P \times P$ block structure defined by the populations, where synaptic weights within a specific block share identical statistical properties (Fig 1(b)). We denote as N_p the number of neurons in population p and $\alpha_p = \frac{N_p}{N}$ the corresponding fraction. The main notations are summarized in Table I.

Following a common approach [29, 32, 34, 36–39, 41],

TABLE I. List of notations.

Notation	Description
i, j	Single neuron indices
p, q	Population indices
N_p	Number of neurons in population p
α_p	Fraction of neurons in population p
J_{pq}^0	Mean synaptic weight from population p to population q
σ_{pq}	standard deviation of the synaptic weights from population p to population q
σ	Re-scaled homogeneous standard deviation of the synaptic weights
$\tau_{pq}^{c/r}$	Correlation coefficient of the chain/reciprocal connectivity motifs
c	Connection probability in sparse networks
J	Excitatory synaptic weights in the sparse E-I network
g	Relative (mean) strength of inhibitory to excitatory synapses in (Gaussian) sparse E-I network
γ	Ratio of inhibitory to excitatory population size

we begin by characterizing connectivity through the marginal distributions $\mathcal{P}(J_{ij} = J)$ of individual synaptic weights, and progressively incorporate higher-order correlations. In this study, we consider the first and second orders, that is, the marginal distribution of individual synaptic weights and the pair-wise correlations. We denote as *motifs* particular pair-wise correlations between synaptic weights (Fig 1(c)). We specifically focus on *chain motifs* corresponding to correlations τ_{ijk}^c between synapses J_{ij} and J_{jk} which share the intermediate neuron j , but $i \neq k$:

$$\tau_{ijk}^c = \frac{[J_{ij}J_{jk}] - [J_{ij}][J_{jk}]}{\sqrt{[(J_{ij} - [J_{ij}])^2][(J_{jk} - [J_{jk}])^2]}}. \quad (1)$$

Here, and throughout this study, square brackets denote the average over the full connectivity distribution.

We contrast the effects of chain motifs with reciprocal motifs corresponding to correlations τ_{ij}^r between connections J_{ij} and J_{ji} [33]:

$$\tau_{ij}^r = \frac{[J_{ij}J_{ji}] - [J_{ij}][J_{ji}]}{\sqrt{[(J_{ij} - [J_{ij}])^2][(J_{ji} - [J_{ji}])^2]}}. \quad (2)$$

Previous studies have considered two additional types of correlations corresponding to convergent and divergent motifs. We show in Appendix A that, in the limit of large networks, they do not contribute to the dynamics we study here.

Because of the assumed population structure, the marginal distributions $\mathcal{P}(J_{ij})$, and the correlation coefficients τ_{ijk}^c and τ_{ij}^r depend only on the populations p, q and s to which the neurons i, j and k belong, so that

$$\begin{aligned} \mathcal{P}(J_{ij} = J) &= f^{pq}(J), \\ \tau_{ijk}^c &= \tau_{pqs}^c, \\ \tau_{ij}^r &= \tau_{pq}^r. \end{aligned} \quad (3)$$

Here $p, q, s \in \{1 \dots P\}$ (Fig 1(a, b)), and $f^{pq}(J)$ is the marginal distribution of synaptic weights from population p to population q .

The connectivity matrix \mathbf{J} can in general be split into a sum of its mean and random parts

$$\mathbf{J} = \mathbf{J}^0 + \mathbf{Z} \quad (4)$$

where $J_{ij}^0 = [J_{ij}]$ are mean connectivity weights and $z_{ij} = J_{ij} - [J_{ij}]$ the zero-mean random part [33].

These two parts are characterized by statistics

$$\begin{aligned} J_{ij}^0 &= J_{pq}^0 \\ [z_{ij}^2] &= \sigma_{pq}^2 \\ \frac{[z_{ij}z_{jk}]}{\sqrt{[z_{ij}^2][z_{jk}^2]}} &= \tau_{pqs}^c \\ \frac{[z_{ij}z_{ji}]}{\sqrt{[z_{ij}^2][z_{ji}^2]}} &= \tau_{pq}^r \end{aligned} \quad (5)$$

where neurons with indexes i, j, k belong to populations p, q and s respectively and $i \neq k$. The mean matrix \mathbf{J}^0 therefore has a $P \times P$ block structure, where entries within each block are identical, so that its rank is $R_0 \leq P$. In contrast, the random component \mathbf{Z} is in general of rank N . The statistics of its entries however exhibit a block-like structure, where variances σ_{pq}^2 and reciprocal correlation coefficients τ_{pq}^r define $P \times P$ matrices, while the chain correlation coefficients $\tau_{c,pqs}$ define a $P \times P \times P$ tensor. Both τ_{pqs}^c and τ_{pq}^r range from -1 to 1 . We further simplify the parameters by assuming that the chain correlation coefficient depends only on the populations of the pre-synaptic neurons of the two synapses, consequently, $\tau_{pqs}^c = \tau_{qs}^c$.

B. Network dynamics

Our goal is to examine the effects of local connectivity statistics on the steady-state response to external inputs. We therefore focus on a simple linear network of rate units, where the firing rate r_i of unit i obeys:

$$\tau \frac{d}{dt} r_i(t) = -r_i(t) + \sum_{j=1}^N J_{ij} r_j(t) + I_i^{ext}(t). \quad (6)$$

Here, $-r_i(t)$ is a standard leak term, the second term on the r.h.s. is the recurrent input from other units in the network, and the third term is an external input.

The firing rate dynamics of neurons in vector format can be written as

$$\tau \frac{d}{dt} \mathbf{r}(t) = -\mathbf{r}(t) + \mathbf{J}\mathbf{r}(t) + \mathbf{I}^{ext}(t), \quad (7)$$

so that the steady-state activity is given by

$$\mathbf{r}^* = (\mathbf{1} - \mathbf{J})^{-1} \mathbf{I}^{ext}. \quad (8)$$

Here $\mathbf{1}$ denotes the $N \times N$ identity matrix.

Our aim is to determine how external inputs to different populations affect the steady-state activity. To this end, we will examine the response matrix \mathbf{X} , where the entry χ_{ij} represents the change of the steady-state activity of neuron i resulting from a change in the input current to neuron j :

$$\chi_{ij} = \frac{dr_i}{dI_j^{ext}}. \quad (9)$$

From Eq. (8) we have

$$\mathbf{X} = (\mathbf{1} - \mathbf{J})^{-1}. \quad (10)$$

The diagonal entries of the response matrix, denoted as χ_{ii} , represent the activity change of neuron i in response to the direct external input they receive. When this term is negative, this indicates that the neuron increases (decreases) its firing rate with a decrease (increase) in the external excitatory input. Generalizing the notion of paradoxical responses of inhibitory neurons [10], we denote any negative response as *paradoxical*. We will in particular examine the relation between local connectivity statistics and paradoxical responses.

II. LOW-RANK APPROXIMATION

To determine how connectivity shapes the response function of the network, we perform a low-rank approximation of the connectivity matrix \mathbf{J} (Fig 1(d)):

$$\mathbf{J} \approx \frac{1}{N} \sum_{r=1}^R \mathbf{m}^{(r)} \mathbf{n}^{(r)\top} \quad (11)$$

$$= \frac{1}{N} \mathbf{M} \mathbf{N}^\top \quad (12)$$

Here $\mathbf{m}^{(r)}$ and $\mathbf{n}^{(r)}$ for $r = 1 \dots R$ are N -dimensional vectors, and \mathbf{M} and \mathbf{N} are $N \times R$ matrices obtained by concatenating these vectors.

While there exists a variety of methods for forming a low-rank approximation, here we use a simple truncated eigen-decomposition. We therefore take the vectors $\mathbf{n}^{(r)}$, $\mathbf{m}^{(r)} \in \mathbb{R}^N$ to be respectively the r -th left and right eigenvectors \mathbf{L}_r and \mathbf{R}_r re-scaled by \sqrt{N} :

$$\mathbf{m}^{(r)} = \sqrt{N} \mathbf{R}_r, \quad \mathbf{n}^{(r)} = \lambda_r \sqrt{N} \mathbf{L}_r. \quad (13)$$

Here, the eigenvectors are ordered by the decreasing absolute value of their eigenvalue λ_r , and obey

$$\mathbf{J} \mathbf{R}_r = \mathbf{R}_r \lambda_r, \quad \mathbf{L}_r^\top \mathbf{J} = \lambda_r \mathbf{L}_r^\top, \quad \mathbf{L}_r^\top \mathbf{R}_{r'} = \delta_{rr'}. \quad (14)$$

Additionally, we impose the constraint that \mathbf{R}_r has unit norm. By retaining only the first R eigenmodes we obtain a rank- R approximation that preserves the top R eigenvalues of \mathbf{J} .

From Eq. (8), this leads to a low-rank approximation of the steady state activity

$$\mathbf{r}^* = (\mathbf{1} - \mathbf{M} \mathbf{N}^\top / N)^{-1} \mathbf{I}^{ext}. \quad (15)$$

Using the Woodbury matrix identity, the steady-state activity can be expressed as:

$$\mathbf{r}^* = (\mathbf{1} + \mathbf{M}(\mathbf{1} - \mathbf{\Lambda})^{-1} \mathbf{N}^\top / N) \mathbf{I}^{ext}, \quad (16)$$

where $\mathbf{\Lambda}$ is the $R \times R$ diagonal matrix containing the top R eigenvalues of \mathbf{J} .

In the low-rank approximation, the entries of the linear response matrix are therefore given by

$$\chi_{ij} = \delta_{ij} + \frac{1}{N} \sum_{r=1}^R \frac{m_i^{(r)} n_j^{(r)}}{1 - \lambda_r}, \quad (17)$$

where δ_{ij} is the Kronecker delta. Note that in [35], the response function in networks with chain motifs was computed using a different method, based on a power series expansion and resummation of the matrix inverse in Eq. (10).

To identify the R dominant eigenmodes of \mathbf{J} , we leverage prior results on the eigenspectra of matrices with a low-rank plus random structure similar to Eq.(4). For such matrices, the eigenspectra typically consist of two components in the complex plane. One component is a continuously-distributed bulk determined by \mathbf{Z} , and the other is a set of discrete outliers controlled by the low-rank structure [42–47]. Previous works have examined the influence of local connectivity motifs on the eigenvalue bulk [30, 32, 48, 49]. Here we instead focus on eigenvalue outliers and their associated eigenvectors. Specifically, we take the rank R in our low-rank approximation to be equal to the number of eigenvalue outliers.

In the subsequent section, we identify the impact of chain and reciprocal motifs on the outlying eigenvalues and corresponding eigenvectors, and then use the low-rank approximation to determine their influence on the steady state response of the network.

III. EIGENVALUE OUTLIERS

In this section, we study the impact of chain motifs on outlying eigenvalues of the connectivity matrix. We first outline the general theory for networks consisting of P populations. We then apply it to excitatory-inhibitory networks consisting of two populations, and contrast fully-connected and sparse networks.

A. General approach

To investigate the impact of local motif statistics on eigenvalues, we expand on earlier work on random matrix theory [33, 34, 41, 43, 46, 50]. The main steps of the mathematical derivations are outlined below, details of the derivation are provided in Appendix B.

Our starting point is the fact that the mean connectivity matrix \mathbf{J}^0 of a network with P populations consists of P blocks and is therefore of rank $R_0 \leq P$. Therefore, it can be exactly expressed as

$$\mathbf{J}^0 = \frac{1}{N} \sum_{r=1}^{R_0} \mathbf{m}_0^{(r)} \mathbf{n}_0^{(r)\top} = \frac{1}{N} \mathbf{M}_0 \mathbf{N}_0^\top, \quad (18)$$

where \mathbf{M}_0 and \mathbf{N}_0 are two $\mathbb{R}^{N \times R_0}$ matrices, and their r -th columns correspond to the right and left eigenvectors $\mathbf{m}_0^{(r)}$ and $\mathbf{n}_0^{(r)}$ of \mathbf{J}^0 associated with the non-zero eigenvalue λ_r^0 . The full connectivity matrix \mathbf{J} (Eq.(4)) can therefore be written as

$$\mathbf{J} = \frac{1}{N} \mathbf{M}_0 \mathbf{N}_0^\top + \mathbf{Z}. \quad (19)$$

Any eigenvalue λ of \mathbf{J} satisfies

$$\det(\mathbf{J} - \lambda \mathbf{1}) = 0. \quad (20)$$

After substituting Eq. (19) and applying the matrix determinant lemma, the determinant in Eq. 20 can be expressed as

$$\begin{aligned} \det(\mathbf{M}_0 \mathbf{N}_0^\top / N + \mathbf{Z} - \lambda \mathbf{1}) &= \det(\mathbf{Z} - \lambda \mathbf{1}) \det(\mathbf{1} + \mathbf{N}_0^\top (\mathbf{Z} - \lambda \mathbf{1})^{-1} \mathbf{M}_0 / N) \\ &= \det(\mathbf{Z} - \lambda \mathbf{1}) \frac{1}{\lambda} \det \left(\lambda \mathbf{1} - \frac{1}{N} \mathbf{N}_0^\top (\mathbf{1} - \mathbf{Z} / \lambda)^{-1} \mathbf{M}_0 \right). \end{aligned} \quad (21)$$

To apply the matrix determinant lemma, we assumed that $\mathbf{Z} - \lambda \mathbf{1}$ is invertible, so that the first term on the r.h.s of Eq. (21) is nonzero. This is guaranteed if λ is larger than the radius of the spectrum of \mathbf{Z} , which we refer to as the *bulk*. The zeros of the second term on the r.h.s corresponds to potential eigenvalues generated by the interaction between \mathbf{Z} and the mean connectivity \mathbf{J}^0 . We refer to these eigenvalues as *outliers* when they lie outside of the bulk spectrum. Note that, if the random component $\mathbf{Z} = \mathbf{0}$, the second term yields the non-zero eigenvalues of the pure low-rank mean connectivity \mathbf{J}^0 .

Expanding the matrix inverse $(\mathbf{1} - \mathbf{Z} / \lambda)^{-1}$ in the second term of Eq. (21), we introduce the matrix

$$\mathbf{Q} = \sum_{k=0}^{\infty} \mathbf{N}_0^\top \mathbf{Z}^k \mathbf{M}_0 / (N \lambda^k). \quad (22)$$

This expansion converges for eigenvalues λ that are outside of the bulk because the norm of \mathbf{Z} / λ is smaller than unity in this case. The outliers are then given by the polynomial equation

$$\det(\lambda \mathbf{1} - \mathbf{Q}) = 0. \quad (23)$$

We focus on the realization-averaged λ , involving the averaging of Eq.(23) and, consequently, the averaging of Eq.(22) over \mathbf{Z} , which we denote with square brackets. As we consider networks with only second-order correlations between synaptic weights, $[\mathbf{Z}^k]$ for odd k are zero, and only even terms remain non-zero. For even $k = 2l$, we show that in the limit of large networks, $[\mathbf{Z}^{2l}] \rightarrow [\mathbf{Z}^2]^l$, with higher powers functioning in a sub-dominant way and thus being negligible in the following calculations (see Appendix A).

Applying geometric sequence summation in Eq. (22), we get

$$[\mathbf{Q}] = \frac{1}{N} \mathbf{N}_0^\top \left(\mathbf{1} - \frac{[\mathbf{Z}^2]}{\lambda^2} \right)^{-1} \mathbf{M}_0. \quad (24)$$

The element i, j of $[\mathbf{Z}^2]$ is given by the pair-wise correlations between synapses, and can be expressed as

$$\left[\sum_{k=1}^N z_{ik} z_{kj} \right] = \begin{cases} N \sum_{q=1}^P \alpha_q \sigma_{pq} \sigma_{qs} \tau_{qs}^c, & i \neq j, \\ N \sum_{q=1}^P \alpha_q \sigma_{pq} \sigma_{qp} \tau_{qp}^r, & i = j, \end{cases} \quad (25)$$

where neurons i and j belong to populations p and s , and α_q represents the fraction of neurons in population q .

Eq. (25) shows that diagonal entries of $[\mathbf{Z}^2]$ are determined by the strength of reciprocal motifs, while the non-zero off-diagonal entries are determined by the strength of chain motifs. Thus, the matrix $[\mathbf{Z}^2]$ can be decomposed into a diagonal matrix $\mathbf{D} \in \mathbb{R}^{N \times N}$ and a matrix $\mathbf{O} \in \mathbb{R}^{N \times N}$ consisting of P^2 blocks with constant entries within blocks that are determined by the strength of chain-motifs across the different populations:

$$[\mathbf{Z}^2] = \mathbf{D} + \mathbf{O}. \quad (26)$$

We further express this block matrix as $\mathbf{O} = \mathbf{U}_o \mathbf{V}_o^\top$, where $\mathbf{U}_o, \mathbf{V}_o \in \mathbb{R}^{N \times R_o}$, and R_o represents the rank of \mathbf{O} which is maximally the number of distinct neuron populations P . To compute the matrix inverse $(\mathbf{1} - [\mathbf{Z}^2] / \lambda^2)^{-1}$, we then apply the Woodbury matrix identity, resulting in:

$$\begin{aligned} \left(\mathbf{1} - \frac{[\mathbf{Z}^2]}{\lambda^2} \right)^{-1} &= \frac{1}{\lambda^2} \mathbf{A}^{-1} \mathbf{U}_o \left(\mathbf{1}_{R_o} - \frac{1}{\lambda^2} \mathbf{V}_o^\top \mathbf{A}^{-1} \mathbf{U}_o \right)^{-1} \\ &\quad \cdot \mathbf{V}_o^\top \mathbf{A}^{-1} + \mathbf{A}^{-1} \\ \mathbf{A}^{-1} &= \text{diag} \left(\left\{ \frac{\lambda^2}{\lambda^2 - D_{ii}} \right\} \right) \end{aligned} \quad (27)$$

where $\mathbf{1}_{R_o}$ is an $\mathbb{R}^{R_o \times R_o}$ identity matrix. Substituting the matrix inverse Eq. (27) into Eqs. (24) and (23) yields a polynomial equation for the eigenvalue outliers of the connectivity matrix \mathbf{J} as a function of the first and second-order statistics of synaptic strengths (see Appendix B for details).

B. Fully connected excitatory-inhibitory networks

1. Definition

We first apply our approach to fully connected networks with Gaussian-distributed synaptic strengths. We consider networks consisting of two populations, an excitatory and an inhibitory one, which we denote with indices $p, q \in \{E, I\}$. Their respective sizes are $N_E = \alpha_E N$ and $N_I = \alpha_I N$.

The marginal distribution f^{pq} of synaptic strengths from population q to population p is given by:

$$f^{pq} = \mathcal{N}(J_{pq}^0, \sigma_{pq}^2) \quad (28)$$

where $p, q \in \{E, I\}$. For simplicity, we set $J_{EE}^0 = J_{IE}^0 = J^0$ and $J_{EI}^0 = J_{II}^0 = -gJ^0$, where g is the relative strength of inhibitory synapses with respect to excitatory ones.

The mean synaptic connectivity \mathbf{J}^0 is then of rank $R_0 = 1$, and can be expressed as $\mathbf{J}^0 = \mathbf{m}_0 \mathbf{n}_0^\top / N$, where

$$\begin{aligned} \mathbf{m}_0 &= [1 \dots]^\top \\ \mathbf{n}_0 &= [NJ^0 \dots, -NgJ^0 \dots]^\top, \end{aligned} \quad (29)$$

\mathbf{J}^0 has a unique non-zero eigenvalue

$$\begin{aligned} \lambda_0 &= N_E J^0 - N_I g J^0 \\ &= (\alpha_E - g\alpha_I) J^0 N. \end{aligned} \quad (30)$$

In the following, we will assume that the network is *inhibition-dominated* [17–19, 51], i.e. that $\alpha_E - g\alpha_I \leq 0$, so that $\lambda_0 \leq 0$. We refer to λ_0 as the *unperturbed eigenvalue*.

We moreover consider a situation where the variance σ_{pq}^2 is identical across populations and strong, i.e. proportional to $1/N$, so that the variance of the total input to neurons is $\mathcal{O}(1)$. In this case, we can write

$$\sigma_{pq}^2 = \frac{\sigma^2}{N} \quad (31)$$

and refer to the parameter σ^2 as the *scaled variance*. This scaling ensures that, in absence of correlations between synapses, the connectivity matrix exhibits a random spectrum of radius independent of N and given by σ [45, 52–54]. If $\lambda_0 < -\sigma$, the mean part of the connectivity leads to a negative outlier [42, 45, 47, 55]. In addition to the first-order statistics, we will assume that the synaptic strengths exhibit correlations described by uniform chain-motif statistics τ^c and reciprocal-motif coefficient τ^r defined in Eq.(5). Numerical procedures for generating the corresponding connectivity matrices are described in Appendix C 1.

The equation for the outlying eigenvalues in this homogeneous case is derived in Appendix B 2. In Appendix B 3, we consider the more general situation where the variances are different in blocks connecting different populations.

2. Eigenvalues

Applying the analytical approach outlined in Sec.III A to networks featuring homogeneous chain and reciprocal motifs, in Eq. (25) the $N(N-1)$ off-diagonal entries in $[\mathbf{Z}^2]$ are non-zero, equal and determined by the chain motif strength τ^c , while the N diagonal entries are determined by the reciprocal motif strength τ^r . Altogether, $[\mathbf{Z}^2]$ is a sum of a diagonal matrix and a uniform, unit-rank matrix (Eq. (26)); substituting this into Eq. (27) leads to the following equation for eigenvalue outliers:

$$\lambda^2 - \lambda_0 \lambda - \Delta^2 = 0, \quad (32)$$

where we assumed $\lambda \neq 0$, and

$$\Delta^2 = \sigma^2 \tau^c (N-1) + \sigma^2 \tau^r. \quad (33)$$

This second-order polynomial equation has two solutions

$$\lambda_{1,2} = \frac{\lambda_0 \mp \sqrt{\lambda_0^2 + 4\Delta^2}}{2}. \quad (34)$$

In the following, we refer to Δ as the eigenvalue perturbation strength. Since we assumed $\lambda_0 \leq 0$, for $\Delta = 0$, $\lambda_1 = \lambda_0$ and $\lambda_2 = 0$. As Δ is increased, λ_1 decreases from λ_0 and generates an increasingly negative real outlier, while λ_2 increases from zero and can give rise to a positive real outlier if it emerges from the bulk of the eigenspectrum. For networks with only chain motifs we have

$$\Delta^2 = \sigma^2 \tau^c (N-1), \quad (35)$$

so that the modulus of the perturbed eigenvalues scales as $\sqrt{\tau^c N}$ (Fig 2). In particular, if the network size N is increased at fixed τ^c , the positive eigenvalue emerges from the random bulk and eventually crosses unity. This implies that positive chain motif strengths fundamentally induce an instability in network dynamics, unless they scale inversely with network size, i.e. $\tau^c \sim 1/N$.

For networks with only homogeneous reciprocal motifs τ^r , the eigenvalue perturbation is instead independent of network size and given by

$$\Delta^2 = \sigma^2 \tau^r. \quad (36)$$

In comparison with chain motifs the perturbation term is independent of N , so that reciprocal motifs have a much weaker effect on outlying eigenvalues [33]. This difference can be traced back to Eq. (26), where reciprocal motifs appear only in the N diagonal entries of \mathbf{D} , while chain motifs determine the $N(N-1)$ off-diagonal elements in $\mathbf{U}_o \mathbf{V}_o^\top$, which leads to a factor $N-1$ in Eq.(35). Put otherwise, there are many more possible chain than reciprocal motifs in a circuit.

Altogether, the key result of our analysis is therefore that *chain motifs* generate a positive outlying eigenvalue

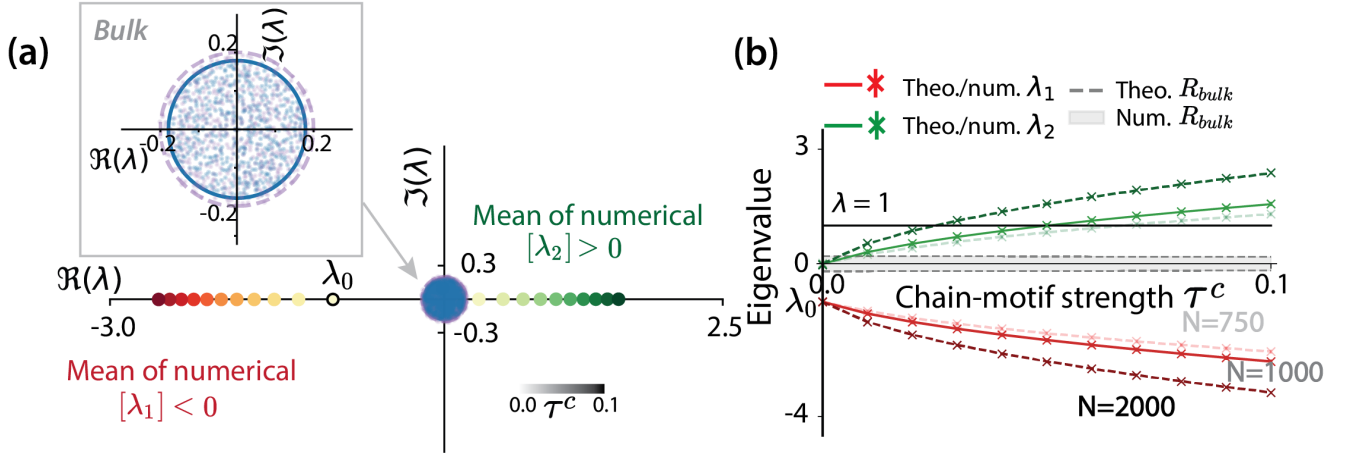


FIG. 2. Impact of chain motifs on the eigenvalues of the connectivity matrix for fully connected excitatory-inhibitory networks. (a) Eigenspectrum in the complex plane. The spectrum consists of a circular bulk (magnification in inset), within which the eigenvalues are continuously distributed, and isolated outliers. Inhibition dominated networks with independent synapses give rise to a single negative outlier λ_0 (black circle). Progressively increasing the strength τ^c of chain motifs (from light to dark), this negative outlier (yellow to red) decreases from the original λ_0 , while an additional positive outlier emerges and increases (light to dark green). The dots show numerically-determined outlying eigenvalues averaged over 30 networks of $N = 1000$ neurons. The inset shows the eigenvalue bulk for a single network realization with $\tau^c = 0$ (purple) and $\tau^c = 0.1$ (blue). (b) Dependence of outlying eigenvalues on the strength τ^c of chain motifs and the network size N . Numerically obtained eigenvalue outliers from 30 network realizations (markers) are shown alongside the theoretical predictions (lines) calculated using Eq.(34). The dominant negative outlier is depicted in red, while the emergent positive outlier is denoted in green. The gray area indicates the radius of the eigenvalue bulk in networks with a size of $N = 1000$, with dashed lines indicating the theoretical values [30]. All parameter values are given in TABLE II.

which increases with network size, and therefore potentially induces an instability by pushing the real part of the outliers above 1, even in otherwise stable, inhibition-dominated networks.

C. Sparse excitatory-inhibitory networks

Next, we turn to sparse excitatory-inhibitory networks and show that chain motifs induce similar outlying eigenvalues to fully-connected networks. We then examine the conditions under which sparsity and excitation-inhibition balance can stabilize the positive outlying eigenvalue.

1. Setup

In sparse networks, only a fraction of possible synaptic connections are non-zero. To define sparse networks with second-order motifs, we start by specifying the first-order statistics of non-zero connections, then add second-order statistics and finally assign synaptic weights to non-zero connections.

As in standard sparse networks [7, 56, 57], the first-order statistics are set by taking any synaptic weight from population q to population p to be non-zero with probability c_{pq} and zero otherwise. Here we assume homogeneous connectivity probabilities $c_{pq} = c$ across populations. The marginal distribution of non-zero connections

is therefore expressed as

$$\begin{aligned} \text{Prob}(J_{ij} \neq 0) &= c, \\ \text{Prob}(J_{ij} = 0) &= 1 - c. \end{aligned} \quad (37)$$

To add chain and reciprocal synaptic motifs, i.e. specific correlations between synapses, we introduce two supplementary parameters ρ^c and ρ^r that define the joint probabilities of non-zero connections across pairs of synapses

$$\begin{aligned} \text{Prob}(J_{ij} \neq 0, J_{jk} \neq 0) &= (1 - \delta_{ik})\rho^c + \delta_{ik}\rho^r, \\ \text{Prob}(J_{ij} = 0, J_{jk} \neq 0) &= (1 - \delta_{ik})(c - \rho^c) + \delta_{ik}(c - \rho^r), \\ \text{Prob}(J_{ij} \neq 0, J_{jk} = 0) &= (1 - \delta_{ik})(c - \rho^c) + \delta_{ik}(c - \rho^r), \\ \text{Prob}(J_{ij} = 0, J_{jk} = 0) &= (1 - \delta_{ik})(1 - c - (c - \rho^c)) \\ &\quad + \delta_{ik}(1 - c - (c - \rho^r)). \end{aligned} \quad (38)$$

We denote the parameters ρ^c and ρ^r as the *occurrence probabilities* for respectively chain and reciprocal motifs. Note that here we implicitly assume a homogeneous motif distribution across different populations. In this framework, independent connections correspond to $\rho^c = c^2$ and $\rho^r = c^2$.

Finally we specify synaptic weights for non-zero synapses. As in the fully connected case, we focus on networks consisting of two populations, an excitatory and an inhibitory one, with respectively $N_E = \alpha_E N$ and $N_I = \alpha_I N$ neurons. For simplicity, we assume that all excitatory and all inhibitory synapses have identical

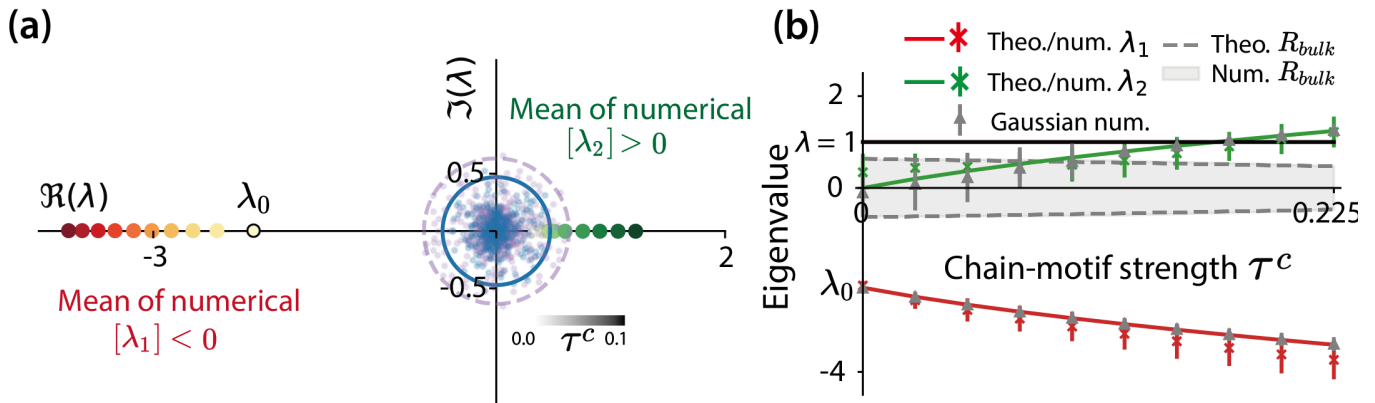


FIG. 3. Impact of chain motifs on the eigenvalues of the connectivity matrix for sparsely connected excitatory-inhibitory networks. (a) Eigenspectrum in the complex plane. Inhibition dominated networks with independent synapses give rise to a single outlier λ_0 (black circle). Progressively increasing the strength τ^c of chain motifs (from light to dark), this negative outlier (yellow to red) decreases from the original λ_0 , while an additional positive outlier emerges and increases (light to dark green). The dots show numerically-determined outlying eigenvalues averaged over 30 networks of $N = 1500$ neurons. The eigenvalue bulk for a single network realization is shown for $\tau^c = 0$ (purple) and $\tau^c = 0.225$ (blue). (b) Dependence of outlying eigenvalues on the strength τ^c of chain motifs. Numerically obtained eigenvalue outliers from 30 network realizations (markers) are shown alongside the theoretical predictions (lines). The dominant negative outlier is depicted in red, while the emergent positive outlier is shown in green. The colored solid lines show the theoretical results calculated using Eqs. (43), (44). The red and green asterisks with error bars represent the results numerically obtained from actual sparse networks (same as subplot (a)), and the gray triangles with error bars represent the results numerically obtained from the equivalent Gaussian networks. The gray area indicates the radius of the eigenvalue bulk in networks with a size of $N = 1500$, with dashed lines indicating the theoretical values ([30] for details). All parameter values are given in TABLE II.

weights, respectively J and $-gJ$ [58], where g represents the ratio of the amplitudes of excitatory synapses to inhibitory synapses.

In practice, we apply the SONET algorithm [34], see Appendix C 2.

2. Gaussian approximation

Previous studies have found that when the distribution of synaptic couplings satisfies the assumptions of the central limit theorem, the spectral properties of the connectivity matrix are well described by Gaussian connectivity with identical first two moments [33, 45, 47, 53, 59]. To determine the outlying eigenvalues in sparse networks with chain motifs, we compute the corresponding first and second moments of the distribution of synaptic weights, and insert them into expressions for the outlying eigenvalues in Gaussian networks. We then compare these analytic predictions with numerical estimations of outlying eigenvalues in sparse networks.

The means and variances of the distributions of synaptic weights for the excitatory and inhibitory populations are given by

$$\begin{aligned} J_{EE}^0 &= J_{EI}^0 = cJ, & \sigma_{EE}^2 &= \sigma_{EI}^2 = c(1-c)J^2 \\ J_{II}^0 &= J_{IE}^0 = -cgJ, & \sigma_{II}^2 &= \sigma_{IE}^2 = c(1-c)g^2J^2. \end{aligned} \quad (39)$$

Using the definitions in Eq.(5), the correlation coefficients of chain motifs between different populations are

given by:

$$\begin{aligned} \tau_{EE}^c &= (\rho^c - c^2)/(c(1-c)), \\ \tau_{EI}^c &= -(\rho^c - c^2)/(c(1-c)), \\ \tau_{IE}^c &= -(\rho^c - c^2)/(c(1-c)), \\ \tau_{II}^c &= (\rho^c - c^2)/(c(1-c)). \end{aligned} \quad (40)$$

Analogously, the correlation coefficients of reciprocal motifs $\tau_{pq}^r, p, q \in \{E, I\}$ are

$$\begin{aligned} \tau_{EE}^r &= (\rho^r - c^2)/(c(1-c)), \\ \tau_{EI}^r &= -(\rho^r - c^2)/(c(1-c)), \\ \tau_{IE}^r &= -(\rho^r - c^2)/(c(1-c)), \\ \tau_{II}^r &= (\rho^r - c^2)/(c(1-c)). \end{aligned} \quad (41)$$

In contrast to fully-connected networks, in sparse networks the mean, variances and correlations of synaptic weights are therefore not independent parameters, but are jointly controlled by the connection probability c , the E and I synaptic weights J and $-gJ$ and the motif occurrence probabilities ρ^c and ρ^r . The relative sign of excitation and inhibition in particular necessarily implies differences in correlation coefficients across different blocks of the connectivity matrix. In addition, the variances also vary across different blocks of the connectivity matrix, while in Sec. III B we assumed all those parameters were homogeneous. An over-representation of EE- and II-type motifs with respect to independent connectivity ($\rho^c, \rho^r > c^2$) yields positive correlation coefficients

$\tau_{EE} = \tau_{II} := +\tau^c$, while an over-representation of EI- and IE-type motifs leads to negative correlation coefficients $\tau_{EI} = \tau_{IE} := -\tau^c$.

Inserting the expressions for the means in Eqs. (30), yields an expression of the outlying eigenvalue in the absence of correlations:

$$\begin{aligned}\lambda_0 &= cN_E J - cN_I g J \\ &= (\alpha_E - g\alpha_I)cJN.\end{aligned}\quad (42)$$

Applying the approach outlined in Sec.III A to networks with heterogeneous variances and correlations leads to expressions for outlying eigenvalues similar to Eq. (34) (Appendix B 3).

$$\lambda_{1,2} = \frac{\lambda_0 \mp \sqrt{\lambda_0^2 + 4\Delta^2}}{2}, \quad (43)$$

where for chain motifs

$$\Delta = JN(\alpha_E - g\alpha_I)\sqrt{c(1-c)\tau^c}. \quad (44)$$

Similarly to fully connected networks, in sparse networks chain motifs therefore lead to the emergence of a positive outlier in inhibition-dominated networks (Fig 3). Comparing Eq. (44) and Eq. (35) reveals that in sparse networks, the eigenvalue perturbation strength scales with N , similarly to fully-connected networks, so that the positive eigenvalue potentially leads to an instability. However in sparse excitatory-inhibitory networks, the perturbation strength also depends on the connection probability strength c and it necessarily contains two opposing terms given by the excitation-inhibition balance $\alpha_E - g\alpha_I$. In the following, we will examine how different assumptions on the connectivity probability and synaptic weights impact the scaling of outlying eigenvalues with the network size N and the stability of the network.

3. Strongly connected regime

We consider first a scaling limit in which the connection probability c and chain motif statistic ρ^c (and therefore τ^c) are independent of N , and the synaptic weight J is of order $1/\sqrt{N}$. This scaling is analogous to the strongly connected regime in networks without motifs [57]. The perturbation term Δ in Eq. (44) then scales as $\sqrt{N}(\alpha_E - g\alpha_I)$. Consequently, the influence of chain motifs on the eigenvalue outliers amplifies with the network size (see Fig 4(a)) and leads to an instability, similarly to our findings in Gaussian networks.

The growth of the perturbation term Δ can only be limited if the balance factor $\alpha_E - g\alpha_I$ scales as $1/\sqrt{N}$. In the strongly connected regime, ensuring network stability thus requires tight balance, with $\alpha_E - g\alpha_I$ approaching zero [9]. This balance requirement also ensures that λ_0 , and the negative outlier, take values independent of network size.

4. Weakly connected regime

We next consider a second type of scaling with network size, where the connection probability c and chain motif occurrence ρ^c decrease with N in such a way that the number C_p of incoming synaptic connections for each neuron, the number of motifs k_{pq}^c and the synaptic strengths J are fixed independently of N . This scaling is analogous to the weakly connected regime in networks without motifs [58]. Here, C_p represents the number of excitatory (if $p = E$) or inhibitory (if $p = I$) synapses targeting the same neuron, while k_{pq}^c denotes the number of chain motifs originating from neurons in population q , passing through neurons in population p and ultimately targeting an individual neuron. These parameters are related to the connection probability c and motif occurrence probability ρ^c via

$$C_p = cN_p, \quad k_{pq}^c = \rho^c N_p N_q, \quad p, q \in \{E, I\}. \quad (45)$$

The weakly connected regime therefore implies that the connection probability scales as $1/N$ and motif occurrence probability as $1/N^2$.

Expressing the eigenvalue perturbation term in Eq. (44) as a function of these parameters, we get

$$\Delta = J(1 - g\frac{\alpha_I}{\alpha_E})\sqrt{(k_{EE}^c - C_E^2)}. \quad (46)$$

In the weakly connected regime, the eigenvalue outliers are therefore independent of the network size N (Fig 4(b)). The stability of the network in the presence of chain motifs is therefore ensured without assuming tight balance between excitation and inhibition.

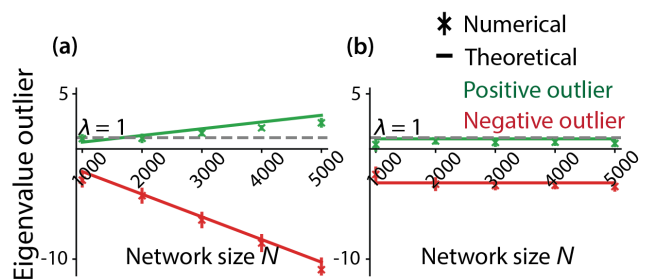


FIG. 4. Dependence of outlying eigenvalues on the network size N ranging from 1000 to 5000 for sparse excitatory-inhibitory connectivity in two different scaling limits. (a) Networks in the strongly connected regime with a constant connectivity probability of $c = 0.2$ and a chain motif probability of $\tau^c = 0.15$ ($\rho^c = 0.064$). (b) Networks in the weakly connected regime with a fixed number of connections and chain motifs, where $C_E = 240$ and $k_{EE}^c = 92160$. The asterisks with error bars indicate the mean and standard deviation of numerically obtained eigenvalue outliers from 30 network instances. Other parameters: $g = 6.8$, $\gamma = 1/4$, $J = 0.0129$.

IV. POPULATION-AVERAGED RESPONSES TO UNIFORM INPUTS

In this section, we use a low-rank approximation of recurrent connectivity to determine how chain motifs affect steady-state responses to external inputs. We focus on population-averaged responses to inputs that are uniform over each population, and specifically examine under which conditions paradoxical responses emerge. We start by outlining the general approach, and then apply it to fully-connected and sparse excitatory-inhibitory networks.

A. Low-rank approximation

Following the approach introduced in Sec. II, we form a low-rank approximation of the connectivity matrix \mathbf{J} by truncating its eigen-decomposition to keep only modes corresponding to the outlying eigenvalues determined in the previous section. We obtain the corresponding left and right connectivity vectors numerically. Within this low-rank approximation, the steady-state response functions of the network are given by Eqs. (15) and (17).

We focus on changes in the average activity of different populations in response to inputs that can differ among populations, but are uniform within each population, so that $I_j^{ext} = I_q^{ext}$ for all j in population q . Averaging Eq. (17) over the connectivity distribution, the mean response χ_{pq} of a neuron i in population p to a uniform input to neurons in population q can be expressed as

$$\chi_{pq} := \left[\sum_{j \in N_q} \chi_{ij} \right] \quad (47)$$

$$= \delta_{pq} + \alpha_q \sum_{r=1}^R \frac{a_{m_r}^p a_{n_r}^q}{1 - \lambda_r}. \quad (48)$$

In the large network limit ($N_p \rightarrow \infty$), where $[\cdot]$ stands for averaging over connectivity. For any vector $\mathbf{x} \in \mathbb{R}^N$, a_x^p is the mean value of its entries within population p :

$$a_x^p = [x_i] \text{ for } i \text{ in population } p. \quad (49)$$

When averaging Eq. (17), we assumed that $m_i^{(r)}$ and $n_j^{(r)}$ are uncorrelated for $i \neq j$ so that $[m_i^{(r)} n_j^{(r)}] = [m_i^{(r)}] [n_j^{(r)}] = a_{m_r}^p a_{n_r}^q$.

Eq. (48) shows that the mean values $a_{m_r}^p$ and $a_{n_r}^q$ are the only statistics of connectivity vectors $\mathbf{m}^{(r)}$ and $\mathbf{n}^{(r)}$ that affect population-averaged responses to uniform inputs. We determine these values numerically by averaging entries of numerically-obtained eigenvectors.

B. Fully connected Gaussian excitatory-inhibitory networks

We start by examining the effect of chain motifs on responses in fully-connected, Gaussian excitatory-inhibitory networks defined in Sec. III B.

In inhibition-dominated networks, we find that the eigenspectrum contains either one or two outliers depending on the strength of chain motifs τ^c (Fig 2). The resulting low-rank approximation is therefore of rank one or two. We refer to the connectivity vectors corresponding to the negative outlier as $\mathbf{m}^{(1)}$ and $\mathbf{n}^{(1)}$. When the connectivity motifs induce a second outlier, we refer to the additional connectivity vectors as $\mathbf{m}^{(2)}$ and $\mathbf{n}^{(2)}$.

Fig 5 shows the mean values of the entries of the connectivity vectors onto excitatory and inhibitory neurons. Increasing τ^c has a weak effect on the mean values of $\mathbf{m}^{(1)}$ (Fig 5 (a), (b)), which remain close to their unperturbed values, but a stronger effect on the mean of $\mathbf{n}^{(1)}$ within the excitatory population (Fig 5 (c)). Remarkably, chain motifs induce comparable mean values for the connectivity vectors $\mathbf{m}^{(2)}$ and $\mathbf{n}^{(2)}$ corresponding to the second outlier. In contrast, eigenvectors corresponding to eigenvalues in the bulk of the eigenspectrum have zero mean (insets in Fig 5).

1. Response to uniform inputs

We first analyze the impact of chain motifs on the average response χ_p of neurons in population p to a uniform input to all neurons in the network.

From Eq. (48), the low-rank approximation for χ_p is given by

$$\chi_p = 1 + \sum_{r=1}^R \frac{a_{m_r}^p}{1 - \lambda_r} \left(\sum_{q \in \{E, I\}} \alpha_q a_{n_r}^q \right). \quad (50)$$

To assess the accuracy of this approximation, we compare it with the steady-state response obtained using the full connectivity matrix \mathbf{J} (Eq. 10). We contrast these values with a prediction based solely on the mean connectivity $\mathbf{J}^0 = \mathbf{m}_0 \mathbf{n}_0^T / N$, for which $a_{m_0}^E = a_{n_0}^I = 1$, $a_{n_0}^E = N J^0$ and $a_{m_0}^I = -N g J^0$ (Eq. (29)), so that

$$\chi_E = \chi_I = \frac{1}{1 - \lambda_0} \quad (51)$$

with $\lambda_0 = (\alpha_E - g \alpha_I) J^0 N$ (Eq. (30)).

While the mean connectivity \mathbf{J}^0 predicts accurately the mean response of random networks without correlations between synapses, we find that including chain motifs strongly amplifies the response of both excitatory and inhibitory populations (Fig 6). This amplification is well captured by the low-rank approximation, which is in excellent agreement with the activity in the

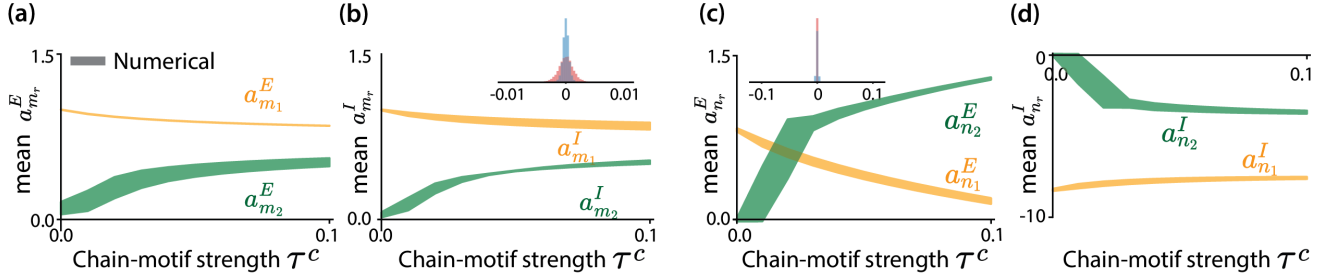


FIG. 5. Impact of chain motifs on population-averaged mean of entries on connectivity vectors for Gaussian networks. (a, b) Population-averaged mean values of entries $m_i^{(r)p}$ on the right connectivity vectors. Subplots (a) and (b) respectively show the mean values for $p = E$ and $p = I$. (c, d) Population-averaged mean values of entries $n_i^{(r)p}$ on the left connectivity vectors. Subplots (c) and (d) respectively show the mean values for $p = E$ and $p = I$. The insets show the distribution of the mean values of the elements in the connectivity vectors corresponding to the eigenvalues in the bulk (red: excitatory population; blue: inhibitory population). The additional eigenvalue emerges from the bulk when $\tau^c = 0.011$. Other network parameters see TABLE II.

full model as τ^c is increased. The accuracy of the low-rank approximation can be explained by the fact that the eigenmodes which correspond to the bulk eigenvalues that were not included in the low-rank description have zero mean components, and therefore do not contribute to the population-averaged response (see insets in Fig 5 (b,c)).

Within the low-rank approximation, we can distinguish the contributions to the response of the two unit-rank terms (Fig 6 colored lines). This decomposition reveals that the unit-rank term associated with the negative outlying eigenvalue has minimal influence on the amplification induced by chain motifs. Conversely, the amplification is due to the second term that corresponds to the newly emerging eigenmode with a positive outlier. The amplification is therefore specific to the outlier induced by chain motifs. In contrast, networks featuring only reciprocal motifs do not give rise to this outlier, and therefore, there is no noticeable amplification as τ^r increases (Fig D.2(a, b)).

2. Paradoxical responses

We next use the low-rank approximation to examine the mean responses χ^{pq} of population p to uniform inputs to population q . Fig 7 shows that chain motifs strongly modulate all components of this response matrix. Focusing on the diagonal entries we denote the response of population p as paradoxical if $\chi_{pp} < 0$, i.e. if it responds in a direction opposite to the input it receives. Fig 7 (d) shows that increasing the strength of chain motifs changes the sign of χ_{II} from positive to negative, thereby switching the response of inhibitory neurons from non-paradoxical in the absence of chain motifs to paradoxical as τ^c is increased.

In networks without correlations between synapses, previous works have shown that the sign of the response of the inhibitory population is controlled by the strength

of the excitatory feedback [10, 12, 13]. Within our framework, the responses in an uncorrelated network are well predicted by using the mean connectivity $\mathbf{J}^0 = \mathbf{m}_0 \mathbf{n}_0^T / N$ in Eq. (48), which leads to:

$$\chi_{II} = \frac{1 - N_E J^0}{1 - \lambda_0}. \quad (52)$$

A paradoxical response of the inhibitory population corresponds to $N_E J^0 > 1$, in agreement with previous results [10, 12, 13]. As the chain motif strength τ^c is gradually increased, the change in the response is dominated by the second term in the low-rank approximation in Eq. (48):

$$\chi_{II} = 1 + \frac{\alpha_I a_{m_1}^I a_{n_1}^I}{1 - \lambda_1} + \frac{\alpha_I a_{m_2}^I a_{n_2}^I}{1 - \lambda_2}. \quad (53)$$

For the inhibitory population, the eigenvector statistics (Fig 5 (d)) show that this second term is negative because $a_{n_2}^I < 0$ and $a_{m_2}^I > 0$. Starting from a non-paradoxical regime with $N_E J^0 < 1$ and $\chi_{II} > 0$, as τ^c is increased, this negative term progressively reduces the value of the response function and eventually leads to a change in the sign of χ_{II} (Fig 7 (d)).

For parameter values used in Fig 7, this change of sign is specific to the response χ_{II} of the inhibitory population. However, because of the large mean values of the unit-rank term corresponding to the positive outlier, τ^c strongly modulates all components of the response.

Our results therefore show that the strength of chain motifs can control whether the network is in a paradoxical regime or not.

C. Sparse excitatory-inhibitory networks

We found that chain motifs have a major impact on responses in fully connected networks. We next inves-

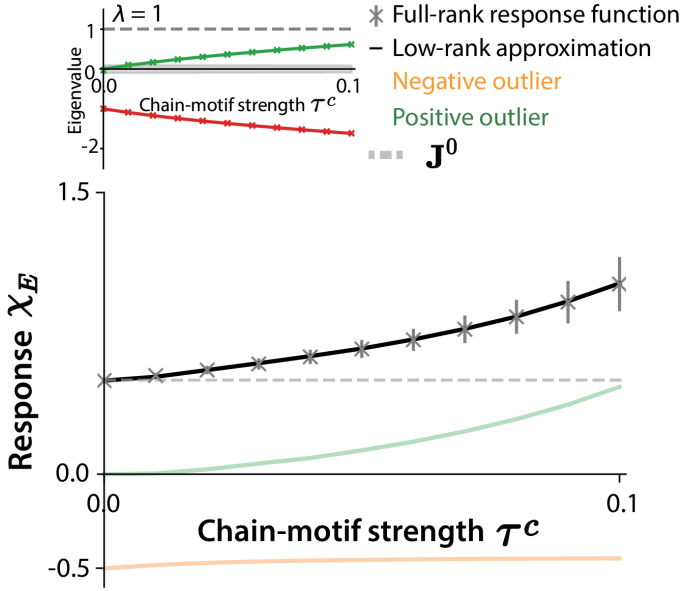


FIG. 6. Impact of chain motifs on the response to uniform external inputs in fully-connected Gaussian excitatory-inhibitory networks: mean response χ_E of the excitatory population as a function of the strength τ^c of chain motifs, which is homogeneous across all blocks of the connectivity matrix. The asterisks with error bars show the mean and s.d. of population-averaged responses in 30 realizations of the full connectivity (Eq. (10)). The lines represent the predictions of the low-rank approximation in Eq. (50), where the a_x^p were obtained numerically by diagonalizing the full connectivity matrix. The dashed line is the prediction obtained from the mean connectivity \mathbf{J}^0 (Eq. (51)). The colored light lines show the respective contributions of the two unit-rank terms in the low-rank approximation of the response (Eq. (50)). Orange and green denote respectively the modes corresponding to the negative and positive outliers. Inset: outlying eigenvalues as a function of τ^c , compared to the bulk of the radius. The positive outlier emerges from the bulk for $\tau^c = 0.011$. All network parameters are given in TABLE II.

tigated to which extent these results extend to sparse networks, where only a fraction of possible synaptic connections are non-zero, and the strength of chain motifs are controlled by the occurrence probability ρ^c (Eq. 38) which then induces different values of the correlation coefficients τ_{pq}^c in different blocks of the connectivity matrix (Eq. 39). More specifically, sparse networks with a uniform occurrence ρ^c of chain motifs examined in Sec. III C lead to correlation coefficients τ_{pq}^c that obey $\tau_{EE}^c = \tau_{II}^c = -\tau_{EI}^c = -\tau_{IE}^c$ (Eq. 39).

As for fully-connected networks, we approximate the sparse connectivity matrix with a low-rank matrix obtained by keeping only the eigenmodes corresponding to the outlying eigenvalues determined in Sec. III C. We compute the corresponding eigenvectors by numerically diagonalizing the sparse connectivity matrix, and then compare their statistics (Fig. 8) with predictions of perturbation theory for Gaussian networks with identical first and second-order connectivity statistics

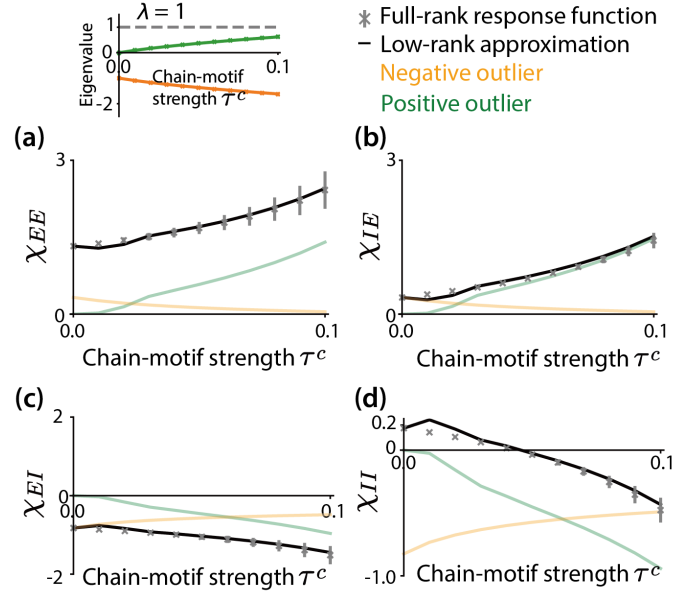


FIG. 7. Impact of chain motifs on the mean response χ_{pq} of population p to uniform inputs to population q , in fully-connected Gaussian excitatory-inhibitory networks. (a) χ_{EE} ; (b) χ_{IE} ; (c) χ_{EI} ; (d) χ_{II} . The asterisks with error bars show the mean and s.d. of population-averaged responses in 30 realizations of the full connectivity (Eq. 10). The solid lines represent the predictions of the low-rank approximation (Eq. (48)), with colored lines indicating the contributions from the two unit rank terms (orange: negative outlier; green: positive outlier). In Eq. (48), a_x^p were obtained numerically by diagonalizing the full connectivity matrix. The strength τ^c of chain motifs is homogeneous across all blocks of the connectivity matrix. The mean connectivity parameters were chosen such that $\chi_{II} > 0$ for $\tau^c = 0$, i.e. the network is in the non-paradoxical regime in absence of inputs. All network parameters are given in TABLE II.

(Sec. III C 2, Fig 8). Note that these eigenvectors are in general not sparse, so that the low-rank approximation of a sparse connectivity matrix is in general not sparse [59].

Similarly to fully-connected networks, increasing the overall strength of chain motifs by increasing ρ^c amplifies the response χ_p to uniform inputs across the network (Fig 9). This effect is well captured by a rank-two approximation, which shows that the amplification is also here due to the positive outlier emerging from the bulk of the eigenspectrum (Fig 9 colored lines).

Inspecting the mean responses χ_{pq} of population p to uniform inputs in population q however revealed important differences between sparse networks (Figs. 10, D.4) and fully connected networks (Fig 7). Indeed, in sparse networks, the mean response of individual populations appeared to change in a direction opposite to fully connected networks when the strength of chain motifs is increased by increasing ρ^c . In particular, the mean response of inhibitory neurons to its inputs increases

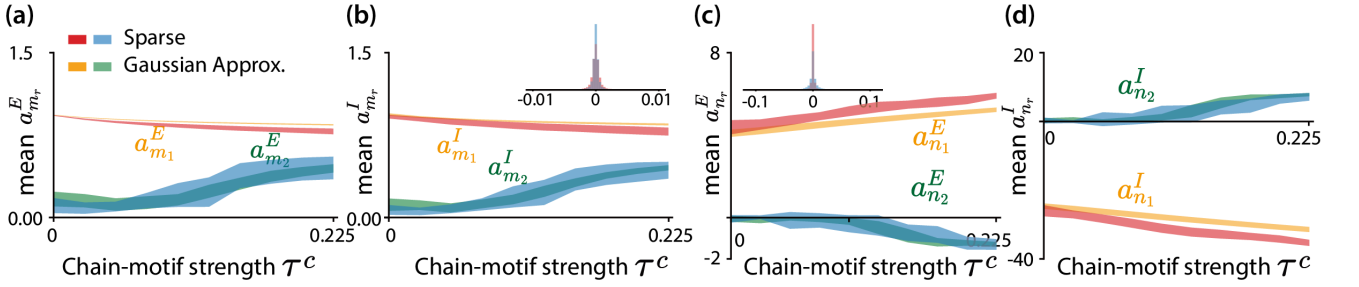


FIG. 8. Impact of chain motifs on population-averaged mean of entries on connectivity vectors for sparse networks (red and blue) and their Gaussian approximations (orange and green). (a, b) Population-averaged mean values of entries $m_i^{(r)p}$ on the right connectivity vectors. Subplots (a) and (b) respectively show the mean values for $p = E$ and $p = I$. (c, d) Population-averaged mean values of entries $n_i^{(r)p}$ on the left connectivity vectors. Subplots (c) and (d) respectively show the mean values for $p = E$ and $p = I$. The insets show the distribution of the mean values of the elements in the connectivity vectors corresponding to the eigenvalues in the bulk (red: excitatory population; blue: inhibitory population). An additional eigenvalue emerges from the bulk $\tau_{EE}^c = 0.11$. For other network parameters see TABLE II.

with $\tau^c := \tau_{EE}^c = \tau_{II}^c = -\tau_{EI}^c = -\tau_{IE}^c$ (Fig 10(d)), while in fully-connected networks it decreases (Fig 7(d)). In sparse networks chain motifs can therefore induce a transition from paradoxical inhibitory responses to non-paradoxical responses (χ_{II} in Fig. D.4), while in fully-connected networks the situation is the opposite. This difference can be traced back to the mean values $a_{m_r}^p$ and $a_{n_r}^p$ of the entries of connectivity vectors that determine the responses χ_{pq} through Eq. 48. Specifically, the mean values $a_{n_2}^E$ and $a_{n_2}^I$ of the second connectivity vector onto the excitatory and inhibitory populations have opposite signs in sparse networks (Figs D.3, 8 (c,d)) compared to fully-connected networks (Fig 5 (c,d)).

D. Effects of chain motif heterogeneity on paradoxical responses

To understand the origin of seemingly opposite effects of chain motifs on paradoxical responses in sparse and fully-connected networks, we note that in fully-connected networks we used homogeneous, positive τ^c , while for sparse networks with a uniform chain motif occurrence ρ^c , the correlation coefficients are different across blocks of the connectivity matrix, with $\tau_{EE}^c = \tau_{II}^c$ positive and $\tau_{EI}^c = \tau_{IE}^c$ negative. We hypothesized that this difference may lead to the distinct dependences of the responses χ_{pq} to the strength of chain motifs. To investigate this possibility, we computed the responses χ_{II} in Gaussian networks where the chain motif strengths were not homogeneous across blocks of the connectivity matrix, but were instead determined by two parameters $\tau_{EE/II}^c$ and $\tau_{EI/IE}^c$ such that $\tau_{EE}^c = \tau_{II}^c = \tau_{EE/II}^c$ and $\tau_{EI}^c = \tau_{IE}^c = \tau_{EI/IE}^c$ (Fig 11). This analysis reconciled the findings in Fig 7 and Fig 10: increasing jointly $\tau_{EE/II}^c = \tau_{EI/IE}^c$ leads to a decreasing response χ_{II} (green line in Fig 11), while setting $\tau_{EE/II}^c = -\tau_{EI/IE}^c$ instead leads to an increase of χ_{II} with the strength of chain motifs (purple line in

Fig 11). We moreover predicted that setting $\tau_{EI/IE}^c = 0$ and increasing $\tau_{EE/II}^c$ would lead to a decreasing χ_{II} , and therefore a switch from a non-paradoxical to a paradoxical response (yellow line and frame in Fig 11). We directly verified this prediction in sparse networks by setting $\rho_{EI/IE}^c = c^2$ and therefore zero correlation coefficients $\tau_{EI/IE}^c = 0$, while maintaining $\tau_{EE/II}^c = \tau^c > 0$ and gradually increasing this value (Fig 11(b) and (c)).

Altogether, our results show that the nature of the response to external inputs strongly, and via explicitly predictable trends, depends on the presence of chain motifs and their distribution across populations.

V. DISCUSSION

Our findings demonstrate that correlations between weights of different synapses, and in particular chain motifs, can exert a dominant impact on the dynamics in networks of recurrently connected neurons. Specifically, our mathematical analyses reveal that even a weak over-representation of chain motifs leads to the emergence of isolated eigenmodes distinct from networks with uncorrelated synaptic weights. In inhibition-dominated networks, these additional eigenmodes are associated with a positive eigenvalue that reflects positive feedback induced by chain motifs. This positive feedback leads to a potential instability that requires revisiting the classical balance conditions.

The positive eigenmode generated by chain motifs strongly contributes to population-averaged responses to external inputs. In particular, we show that through this eigenmode, chain motifs can induce paradoxical responses in networks where such responses are not expected based on mean connectivity alone [10, 15, 19, 60, 61]. Conversely, in inhibition-stabilized networks that exhibit paradoxical responses in the absence of correlations between synapses, chain motifs can shift the dynamics

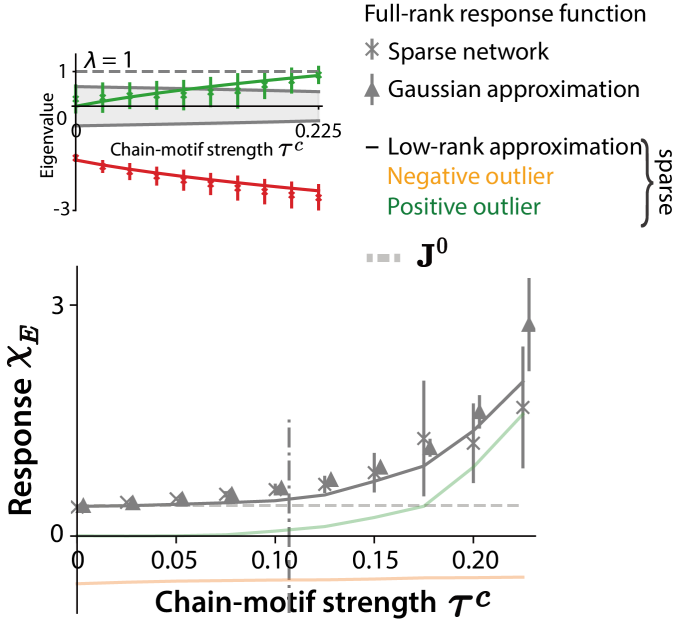


FIG. 9. Impact of chain motifs on the mean response χ_E of excitatory neurons to uniform external inputs in sparse networks, as a function of strength of chain motifs, which is heterogeneous across blocks of the connectivity matrix, with $\tau^c = \tau_{EE}^c = \tau_{II}^c = -\tau_{EI}^c = -\tau_{IE}^c$. The asterisks with error bars show the mean and s.d. of χ_E in 30 realizations of the full sparse network. The triangles with error bars show the mean and s.d. of χ_E in 30 realizations of the equivalent Gaussian approximation. The lines represent the predictions of the low-rank approximation in Eq. (11), where the a_x^p were obtained numerically by diagonalizing the sparse connectivity matrix. The dashed line is the prediction obtained from the mean connectivity \mathbf{J}^0 (Eq. (51)). The colored light lines illustrate the respective contributions of the two unit-rank terms in the low-rank approximation of the response of the sparse networks. Orange and green denote respectively the modes corresponding to the negative and positive outliers. Inset: outlying eigenvalues as a function of τ^c , compared to the bulk of the radius. The positive outlier emerges from the bulk for $\tau^c = 0.11$ (vertical dash-dot line). For other network parameters, see TABLE II.

towards non-paradoxical responses. Mean connectivity therefore does not predict the nature of the responses when chain motifs are present, but we expect that paradoxical responses still correspond to networks where the excitatory sub-network is unstable by itself [15].

Previous works have examined the effects of connectivity motifs on the continuous bulk of the spectrum [30–32, 49, 62]. Here we instead focus on eigenmodes corresponding to eigenvalues that lie outside of the bulk. Our results show that connectivity motifs have distinct effects on these outliers, which determine the responses to external inputs.

The present paper, with its emphasis on spectral properties of networks, complements allied studies on the role of connection motifs on network dynamics [30–40]. Perhaps most related to the present paper is [35], which ex-

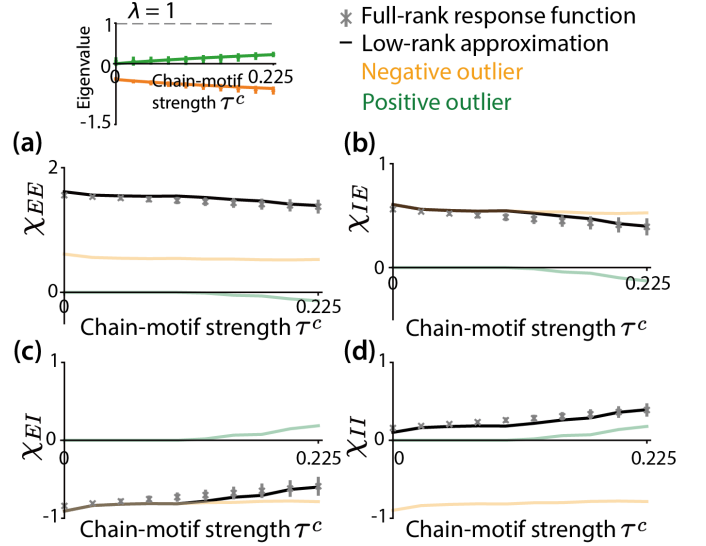


FIG. 10. Impact of chain motifs on the mean response χ_{pq} of population p to uniform inputs to population q , in sparse excitatory-inhibitory networks. The subplots show the same quantities as in Fig 7. The mean connectivity parameters were chosen such that $\chi_{II} > 0$ for $\tau^c = 0$. All network parameters are given in TABLE II.

presses the response function for similar linearized rate networks in terms of a sequence of motif cumulants, which are the occurrences of motif structures at levels over and above what one would expect from the occurrence of their constituent parts. This leads to a general strong role for chains in particular over and above other motifs. The present paper shares this emphasis on the importance of chain motifs, but arrives at this conclusion via different methods based on explicit computations of eigenvalues based on correlations among connections rather than the cumulant-based techniques of [35]. Moreover, here we focus on distinct questions: the impact of chain motifs on stability and paradoxical responses in the ubiquitous setting of balanced E-I networks, and the general interplay among synaptic motifs and larger-scale, low-rank connectivity patterns established by cell-type specific connectivity probabilities.

For the sake of analytical tractability, our study is based on a number of simplifying assumptions. We considered only linear, rate-based dynamics, while a number of previous studies outlined the effects of the non-linearity on paradoxical responses, in particular in supralinear-stabilized networks of excitatory and inhibitory neurons [12–14, 63, 64]. Although a full non-linear analysis of N -dimensional networks with correlated synapses is in general untractable, networks with low-rank connectivity allow for an exact low-dimensional reduction even in the presence of non-linearities [42, 65, 66]. Applying the low-rank approximation of correlated connectivity to supralinear stabilized networks is therefore an interesting direction for future research. Beyond rate-

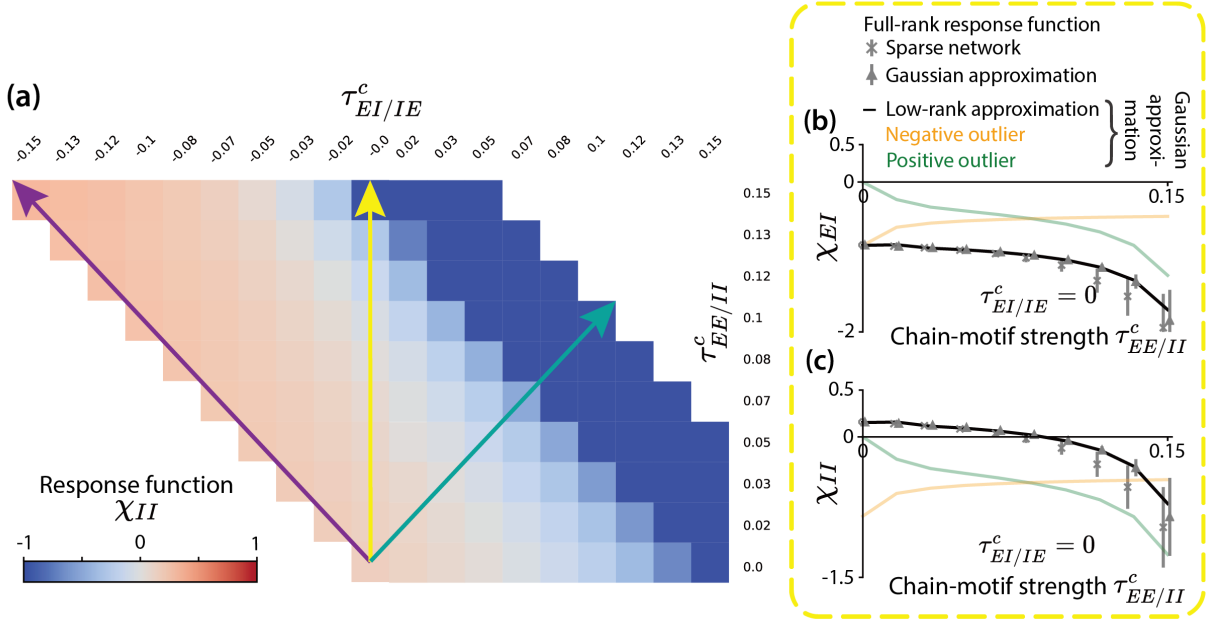


FIG. 11. Impact of the heterogeneity of chain motifs on the response to external inputs. (a) Response χ_{II} of inhibitory neurons as a function of $\tau^c_{EE/II} = \tau^c_{EE} = \tau^c_{II}$ and $\tau^c_{EI/IE} = \tau^c_{EI} = \tau^c_{IE}$, for the fully connected Gaussian approximation of sparse networks. The green line corresponds to homogeneous chain motifs ($\tau^c_{EE} = \tau^c_{II} = \tau^c_{EI} = \tau^c_{IE}$), for which the response is shown in Fig 7. The purple line corresponds to homogeneous chain motifs occurrence ρ^C , leading to $\tau^c_{EE} = \tau^c_{II} = -\tau^c_{EI} = -\tau^c_{IE}$, for which the response is shown in Fig 10. The yellow line shows the prediction for networks with $\tau^c_{EI/IE} = 0$. (b) Response function χ_{EI} and (c) response function χ_{II} in sparse networks and corresponding fully connected Gaussian approximations with $\tau^c_{EI/IE} = 0$. Details of subplots (b) and (c) are identical to Fig 10. The other network parameters are identical to Fig 10.

based models, numerical analyses of integrate-and-fire networks with low-rank connectivity structure suggest that the analytical insights from rate networks extend to spiking networks [67].

In this work, we focused on networks of only two populations, with the additional constraint that the mean connectivity \mathbf{J}^0 is unit rank. As a consequence, the mean connectivity induces a single eigenmode, which in inhibition-dominated networks corresponds to a negative outlying eigenvalue. Our key result is that in this situation chain motifs lead to an additional eigenmode with a positive outlying eigenvalue. Relaxing the unit-rank constraint, and increasing the number of populations leads to additional non-trivial eigenmodes of the mean connectivity \mathbf{J}^0 , and additional outlying eigenvalues induced by chain motifs. Systematically mapping the resulting eigenspectrum configurations is left for future work. It would be particularly interesting to examine the effects of multiple inhibitory sub-types and their interactions with synaptic motifs.

Altogether, our results argue for the importance of moving beyond the classical paradigm of excitatory-inhibitory networks with uncorrelated synaptic weights. These models have been instrumental for generating mechanistic interpretations of neural recordings, in particular for spontaneous activity [7, 8, 57, 58] and responses to external inputs [11, 13, 14, 20, 21, 68, 69]. Yet

they strongly rely on the assumption that the strengths of different synapses are statistically independent and therefore determined by their mean and variance. Experimental recordings of synaptic weights clearly show that individual synapses are not independent, and our study demonstrates that basic correlations can have strong effects on dynamics, both in terms of stability and the nature of responses to inputs. More generally, the computations performed by networks of neurons in the brain stem from the structure in the connections at both the large scale of cell-type averages and the smaller scale of synaptic configurations beyond these averages, and the analytical approach developed here offers a way of combining these levels of description to advance the links between connectivity structure and the dynamics of computation.

DATA AVAILABILITY

The code for all simulations and figure generation will be available on GitHub upon publication of the paper.

ACKNOWLEDGMENTS

YS and SO were supported by the Eranet-Neuron project IMBALANCE and the program “Ecoles Universitaires de Recherche” launched by the French Government and implemented by the ANR, with the reference ANR-17-EURE-0017. YS was supported by the National Nat-

ural Science Foundation of China (grant no. 32400936), the Fundamental Research Funds for the Central Universities (grant no. 2233100030), the NSF AccelNet IN-BIC program (grant No. OISE-2019976). DD was funded by the Deutsche Forschungsgemeinschaft (DFG, German Research Foundation) as part of the SPP 2205 – 533396241. We additionally acknowledge partial support of NIH grant R01 1RF1DA055669. We thank K.D. Miller for comments on the manuscript.

-
- [1] R. J. Douglas and K. A. Martin, Neuronal circuits of the neocortex, *Annu. Rev. Neurosci.* **27**, 419 (2004).
- [2] K. D. Harris and T. D. Mrsic-Flogel, Cortical connectivity and sensory coding, *Nature* **503**, 51 (2013).
- [3] K. D. Harris and G. M. Shepherd, The neocortical circuit: themes and variations, *Nature neuroscience* **18**, 170 (2015).
- [4] L. Luo, Architectures of neuronal circuits, *Science* **373**, eabg7285 (2021).
- [5] M. N. Shadlen and W. T. Newsome, Noise, neural codes and cortical organization, *Current opinion in neurobiology* **4**, 569 (1994).
- [6] M. N. Shadlen and W. T. Newsome, The variable discharge of cortical neurons: implications for connectivity, computation, and information coding, *Journal of neuroscience* **18**, 3870 (1998).
- [7] C. Van Vreeswijk and H. Sompolinsky, Chaos in neuronal networks with balanced excitatory and inhibitory activity, *Science* **274**, 1724 (1996).
- [8] D. J. Amit and N. Brunel, Model of global spontaneous activity and local structured activity during delay periods in the cerebral cortex., *Cerebral cortex (New York, NY: 1991)* **7**, 237 (1997).
- [9] G. Hennequin, E. J. Agnes, and T. P. Vogels, Inhibitory plasticity: balance, control, and codependence, *Annual review of neuroscience* **40**, 557 (2017).
- [10] M. V. Tsodyks, W. E. Skaggs, T. J. Sejnowski, and B. L. McNaughton, Paradoxical effects of external modulation of inhibitory interneurons, *Journal of neuroscience* **17**, 4382 (1997).
- [11] H. Ozeki, I. M. Finn, E. S. Schaffer, K. D. Miller, and D. Ferster, Inhibitory stabilization of the cortical network underlies visual surround suppression, *Neuron* **62**, 578 (2009).
- [12] A. Litwin-Kumar, R. Rosenbaum, and B. Doiron, Inhibitory stabilization and visual coding in cortical circuits with multiple interneuron subtypes, *Journal of neurophysiology* **115**, 1399 (2016).
- [13] D. B. Rubin, S. D. Van Hooser, and K. D. Miller, The stabilized supralinear network: a unifying circuit motif underlying multi-input integration in sensory cortex, *Neuron* **85**, 402 (2015).
- [14] Y. Ahmadian, D. B. Rubin, and K. D. Miller, Analysis of the stabilized supralinear network, *Neural computation* **25**, 1994 (2013).
- [15] K. D. Miller and A. Palmigiano, Generalized paradoxical effects in excitatory/inhibitory networks, *BioRxiv*, 2020 (2020).
- [16] S. Sadeh and C. Clopath, Inhibitory stabilization and cortical computation, *Nature Reviews Neuroscience* **22**, 21 (2021).
- [17] G. Hennequin, Y. Ahmadian, D. B. Rubin, M. Lengyel, and K. D. Miller, The dynamical regime of sensory cortex: stable dynamics around a single stimulus-tuned attractor account for patterns of noise variability, *Neuron* **98**, 846 (2018).
- [18] Y. Ahmadian and K. D. Miller, What is the dynamical regime of cerebral cortex?, *Neuron* **109**, 3373 (2021).
- [19] A. Sanzeni, B. Akitake, H. C. Goldbach, C. E. Leedy, N. Brunel, and M. H. Histed, Inhibition stabilization is a widespread property of cortical networks, *Elife* **9**, e54875 (2020).
- [20] A. Palmigiano, F. Fumarola, D. P. Mossing, N. Kravnyukova, H. Adesnik, and K. D. Miller, Common rules underlying optogenetic and behavioral modulation of responses in multi-cell-type v1 circuits, *bioRxiv*, 2020 (2020).
- [21] A. Sanzeni, A. Palmigiano, T. H. Nguyen, J. Luo, J. J. Nassi, J. H. Reynolds, M. H. Histed, K. D. Miller, and N. Brunel, Mechanisms underlying reshuffling of visual responses by optogenetic stimulation in mice and monkeys, *Neuron* **111**, 4102 (2023).
- [22] M. Winding, B. D. Pedigo, C. L. Barnes, H. G. Patso-lic, Y. Park, T. Kazimiers, A. Fushiki, I. V. Andrade, A. Khandelwal, J. Valdes-Aleman, *et al.*, The connectome of an insect brain, *Science* **379**, eadd9330 (2023).
- [23] L. Campagnola, S. C. Seeman, T. Chartrand, L. Kim, A. Hoggarth, C. Gamlin, S. Ito, J. Trinh, P. Davoudian, C. Radaelli, *et al.*, Local connectivity and synaptic dynamics in mouse and human neocortex, *Science* **375**, eabj5861 (2022).
- [24] C. K. Pfeffer, M. Xue, M. He, Z. J. Huang, and M. Scanziani, Inhibition of inhibition in visual cortex: the logic of connections between molecularly distinct interneurons, *Nature neuroscience* **16**, 1068 (2013).
- [25] S. Lefort, C. Tomm, J.-C. F. Sarria, and C. C. Petersen, The excitatory neuronal network of the c2 barrel column in mouse primary somatosensory cortex, *Neuron* **61**, 301 (2009).
- [26] S. B. Hofer, H. Ko, B. Pichler, J. Vogelstein, H. Ros, H. Zeng, E. Lein, N. A. Lesica, and T. D. Mrsic-Flogel, Differential connectivity and response dynamics of excitatory and inhibitory neurons in visual cortex, *Nature neuroscience* **14**, 1045 (2011).
- [27] Y. Peng, F. X. Mittermaier, H. Planert, U. C. Schneider, H. Alle, and J. R. P. Geiger, High-throughput microcircuit analysis of individual human brains through next-

- generation multineuron patch-clamp, *Elife* **8**, e48178 (2019).
- [28] P. Rupprecht and R. W. Friedrich, Precise synaptic balance in the zebrafish homolog of olfactory cortex, *Neuron* **100**, 669 (2018).
- [29] S. Song, P. J. Sjöström, M. Reigl, S. Nelson, and D. B. Chklovskii, Highly nonrandom features of synaptic connectivity in local cortical circuits, *PLoS biology* **3**, e68 (2005).
- [30] D. Dahmen, S. Recanatesi, G. K. Ocker, X. Jia, M. Helias, and E. Shea-Brown, Strong coupling and local control of dimensionality across brain areas, *Biorxiv*, 2020 (2020).
- [31] D. Martí, N. Brunel, and S. Ostojic, Correlations between synapses in pairs of neurons slow down dynamics in randomly connected neural networks, *Physical Review E* **97**, 062314 (2018).
- [32] Y. Hu and H. Sompolinsky, The spectrum of covariance matrices of randomly connected recurrent neuronal networks with linear dynamics, *PLoS computational biology* **18**, e1010327 (2022).
- [33] Y. Shao and S. Ostojic, Relating local connectivity and global dynamics in recurrent excitatory-inhibitory networks, *PLOS Computational Biology* **19**, e1010855 (2023).
- [34] L. Zhao, B. Beverlin, T. Netoff, and D. Q. Nykamp, Synchronization from second order network connectivity statistics, *Frontiers in computational neuroscience* **5**, 28 (2011).
- [35] Y. Hu, S. L. Brunton, N. Cain, S. Mihalas, J. N. Kutz, and E. Shea-Brown, Feedback through graph motifs relates structure and function in complex networks, *Physical Review E* **98**, 062312 (2018).
- [36] J. Trousdale, Y. Hu, E. Shea-Brown, and K. Josić, Impact of network structure and cellular response on spike time correlations, *PLoS computational biology* **8**, e1002408 (2012).
- [37] Y. Hu, J. Trousdale, K. Josić, and E. Shea-Brown, Motif statistics and spike correlations in neuronal networks, *Journal of Statistical Mechanics: Theory and Experiment* **2013**, P03012 (2013).
- [38] Y. Hu, J. Trousdale, K. Josić, and E. Shea-Brown, Local paths to global coherence: Cutting networks down to size, *Physical Review E* **89**, 032802 (2014).
- [39] G. K. Ocker, K. Josić, E. Shea-Brown, and M. A. Buice, Linking structure and activity in nonlinear spiking networks, *PLoS computational biology* **13**, e1005583 (2017).
- [40] S. Recanatesi, G. Ocker, M. Buice, and E. Shea-Brown, Dimensionality in recurrent spiking networks: Global trends in activity and local origins in connectivity, *PLoS Computational Biology* **15**, e1006446 (2019).
- [41] D. Q. Nykamp, Revealing pairwise coupling in linear-nonlinear networks, *SIAM Journal on Applied Mathematics* **65**, 2005 (2005).
- [42] F. Mastrogiuseppe and S. Ostojic, Linking connectivity, dynamics, and computations in low-rank recurrent neural networks, *Neuron* **99**, 609 (2018).
- [43] F. Schuessler, A. Dubreuil, F. Mastrogiuseppe, S. Ostojic, and O. Barak, Dynamics of random recurrent networks with correlated low-rank structure, *Physical Review Research* **2**, 013111 (2020).
- [44] L. Logiaco, L. Abbott, and S. Escola, Thalamic control of cortical dynamics in a model of flexible motor sequencing, *Cell reports* **35** (2021).
- [45] K. Rajan and L. F. Abbott, Eigenvalue spectra of random matrices for neural networks, *Physical review letters* **97**, 188104 (2006).
- [46] T. Tao, Outliers in the spectrum of iid matrices with bounded rank perturbations, *Probability Theory and Related Fields* **155**, 231 (2013).
- [47] D. Dahmen, S. Grün, M. Diesmann, and M. Helias, Second type of criticality in the brain uncovers rich multiple-neuron dynamics, *Proceedings of the National Academy of Sciences* **116**, 13051 (2019).
- [48] J. Aljadeff, M. Stern, and T. Sharpee, Transition to chaos in random networks with cell-type-specific connectivity, *Physical review letters* **114**, 088101 (2015).
- [49] A. Kuczala and T. O. Sharpee, Eigenvalue spectra of large correlated random matrices, *Physical Review E* **94**, 050101 (2016).
- [50] A. Greenbaum, R.-c. Li, and M. L. Overton, First-order perturbation theory for eigenvalues and eigenvectors, *SIAM review* **62**, 463 (2020).
- [51] T. P. Vogels, H. Sprekeler, F. Zenke, C. Clopath, and W. Gerstner, Inhibitory plasticity balances excitation and inhibition in sensory pathways and memory networks, *Science* **334**, 1569 (2011).
- [52] A. Edelman and N. R. Rao, Random matrix theory, *Acta numerica* **14**, 233 (2005).
- [53] J. Kadmon and H. Sompolinsky, Transition to chaos in random neuronal networks, *Physical Review X* **5**, 041030 (2015).
- [54] T. Tao, *Topics in random matrix theory*, Vol. 132 (American Mathematical Society, 2023).
- [55] S. Ostojic, Two types of asynchronous activity in networks of excitatory and inhibitory spiking neurons, *Nature neuroscience* **17**, 594 (2014).
- [56] I. Ginzburg and H. Sompolinsky, Theory of correlations in stochastic neural networks, *Physical review E* **50**, 3171 (1994).
- [57] A. Renart, J. De La Rocha, P. Bartho, L. Hollender, N. Parga, A. Reyes, and K. D. Harris, The asynchronous state in cortical circuits, *science* **327**, 587 (2010).
- [58] N. Brunel, Dynamics of sparsely connected networks of excitatory and inhibitory spiking neurons, *Journal of computational neuroscience* **8**, 183 (2000).
- [59] E. Herbert and S. Ostojic, The impact of sparsity in low-rank recurrent neural networks, *PLOS Computational Biology* **18**, e1010426 (2022).
- [60] L. C. Garcia del Molino, G. R. Yang, J. F. Mejias, and X.-J. Wang, Paradoxical response reversal of top-down modulation in cortical circuits with three interneuron types, *Elife* **6**, e29742 (2017).
- [61] S. Sadeh and C. Clopath, Patterned perturbation of inhibition can reveal the dynamical structure of neural processing, *Elife* **9**, e52757 (2020).
- [62] M. Layer, M. Helias, and D. Dahmen, Effect of synaptic heterogeneity on neuronal coordination, *P R X Life* **2**, 013013 (2024).
- [63] Y. K. Wu and J. Gjorgjieva, Inhibition stabilization and paradoxical effects in recurrent neural networks with short-term plasticity, *Physical Review Research* **5**, 033023 (2023).
- [64] C. J. Holt, K. D. Miller, and Y. Ahmadian, The stabilized supralinear network accounts for the contrast dependence of visual cortical gamma oscillations, *PLOS Computational Biology* **20**, e1012190 (2024).

- [65] M. Beiran, A. Dubreuil, A. Valente, F. Mastrogiuseppe, and S. Ostoic, Shaping dynamics with multiple populations in low-rank recurrent networks, *Neural Computation* **33**, 1572 (2021).
- [66] A. Dubreuil, A. Valente, M. Beiran, F. Mastrogiuseppe, and S. Ostoic, The role of population structure in computations through neural dynamics, *Nature neuroscience* **25**, 783 (2022).
- [67] L. Cimeša, L. Ciric, and S. Ostoic, Geometry of population activity in spiking networks with low-rank structure, *PLoS Computational Biology* **19**, e1011315 (2023).
- [68] B. K. Murphy and K. D. Miller, Balanced amplification: a new mechanism of selective amplification of neural activity patterns, *Neuron* **61**, 635 (2009).
- [69] L. Hertäg and H. Sprekeler, Learning prediction error neurons in a canonical interneuron circuit, *Elife* **9**, e57541 (2020).
- [70] F. Chung and L. Lu, Connected components in random graphs with given expected degree sequences, *Annals of combinatorics* **6**, 125 (2002).

Appendix A: Other second-order motifs

In the main text, we focus on the chain and reciprocal motifs, however two other types of second-order motifs can be distinguished: divergent and convergent motifs (Fig. 1(c)). Divergent motifs correspond to the correlation coefficient τ_{ikj}^{div} between synapses J_{ij} and J_{kj} which share an identical pre-synaptic neuron j but have different post-synaptic neurons $i \neq k$:

$$\tau_{ikj}^{div} = \frac{[J_{ij}J_{kj}] - [J_{ij}][J_{kj}]}{\sqrt{[(J_{ij} - [J_{ij}])^2][(J_{kj} - [J_{kj}])^2]}} = \frac{[z_{ij}z_{kj}]}{\sqrt{[z_{ij}^2][z_{kj}^2]}}; \quad (\text{A1})$$

Convergent motifs correspond to the correlation coefficient τ_{ikj}^{con} between synapses J_{ik} and J_{ij} which share the identical post-synaptic neuron i but have different pre-synaptic neurons $j \neq k$:

$$\tau_{ikj}^{con} = \frac{[J_{ik}J_{ij}] - [J_{ik}][J_{ij}]}{\sqrt{[(J_{ik} - [J_{ik}])^2][(J_{ij} - [J_{ij}])^2]}} = \frac{[z_{ik}z_{ij}]}{\sqrt{[z_{ik}^2][z_{ij}^2]}}. \quad (\text{A2})$$

$$\begin{aligned} [(\mathbf{Z}^2)_{ij} (\mathbf{Z}^2)_{jk}] &= \sum_{s,l}^N [z_{is}z_{sj}z_{jl}z_{lk}] \\ &= \sum_{s,l}^N ([z_{is}z_{sj}][z_{jl}z_{lk}] + [z_{is}z_{jl}][z_{sj}z_{lk}] + [z_{is}z_{lk}][z_{jl}z_{sj}]) \\ &= [\mathbf{Z}^2]_{ij} [\mathbf{Z}^2]_{jk} + \sum_s^N [z_{is}z_{js}][z_{sj}z_{sk}] + \sum_s^N [z_{is}z_{sk}][z_{js}z_{sj}] \\ &= [\mathbf{Z}^2]_{ij} [\mathbf{Z}^2]_{jk} + N\tau^{con}\sigma_z^2\tau^{div}\sigma_z^2 + N\tau^c\sigma_z^2\tau^r\sigma_z^2. \end{aligned} \quad (\text{A3})$$

We used Wick's theorem from the first line to the second line. From the second line to the third line, we used $i \neq j \neq k$. We moreover assumed $[z_{is}z_{jl}] = 0$ unless two of the pre-synaptic neuron indices are identical, so that the second and third terms are non-zero only when $s = l$. Since (Eq. (25))

$$[\mathbf{Z}^2]_{ij} = N\tau^c\sigma_z^2, \quad i \neq j \quad (\text{A4})$$

we have,

$$\begin{aligned} \frac{[(\mathbf{Z}^2)_{ij} (\mathbf{Z}^2)_{jk}]}{[\mathbf{Z}^2]_{ij} [\mathbf{Z}^2]_{jk}} &= 1 + \frac{N\tau^{div}\tau^{con}\sigma_z^4 + N\tau^c\tau^r\sigma_z^4}{(N^2\tau^c)^2\sigma_z^4} \\ &= 1 + \mathcal{O}(N^{-1}). \end{aligned} \quad (\text{A5})$$

The correlation between fluctuations in $(\mathbf{Z}^2)_{ij}$ and $(\mathbf{Z}^2)_{jk}$ diminishes with a scaling factor of $1/N$. This correlation tends to vanish in the limit of a large network as N approaches infinity.

Only chain and reciprocal motifs contribute to the dynamics for large N because they correspond to elements of the matrix $[\mathbf{Z}^2]$ (Eq. (25)) that determines the outlying eigenvalues. In contrast, divergent and convergent motifs do not affect the matrix $[\mathbf{Z}^2]$, but they contribute to higher powers $[\mathbf{Z}^{2k}]$ in a sub-dominant fashion. To illustrate this higher-order impact, we consider a single population network with homogeneous motif strengths $\tau^c, \tau^r, \tau^{div}, \tau^{con}$ and a homogeneous variance of \mathbf{Z} , denoted by σ_z^2 , and calculate $[\mathbf{Z}^4]$ as an example. Computing the product of two entries $(\mathbf{Z}^2)_{ij}, (\mathbf{Z}^2)_{jk}, i \neq j \neq k$, its average is expressed as

Appendix B: Eigenvalue calculations

1. General approach

Using the determinant lemma (Eq. (19)-(21)) we show that the eigenvalues of matrix \mathbf{J} after perturbations are the solutions of the characteristic polynomial of the matrix \mathbf{Q} (Eq. (22)). As $[\mathbf{Z}^k] = 0$ for odd k , the realization average of \mathbf{Q} is given by

$$[\mathbf{Q}] = \sum_{l=0}^{\infty} \mathbf{N}_0^T [\mathbf{Z}^{2l}] \mathbf{M}_0 / (N\lambda^{2l}) \quad (\text{B1})$$

In general, $[\mathbf{Z}^{2l}] \neq [\mathbf{Z}^2]^l$, however, the correlation between entries $(\mathbf{Z}^2)_{ij}$ and $(\mathbf{Z}^2)_{jk}$ vanishes in the large network limit $N \rightarrow \infty$ (Appendix A).

TABLE II. List of simulation parameters.

Parameters	Simulations					
	Figs 2,D.1(a)	Figs 5,6, D.2(a)	Fig D.1(b)	Figs 3, D.1(c)	Figs 8,9, D.2(b),D.4	Figs 10,11 D.3
N	1000	1000	1000	1500	1500	1500
J^0	$8.125 \times 1E-4$	$8.125 \times 1E-4$	$8.125 \times 1E-4$	-	-	-
σ	0.2	0.1	0.5	-	-	-
g	10.15	10.15	10.15	6.8	6.0	6.0
γ	1/4	1/4	1/4	1/4	1/4	1/4
c	-	-	-	0.2	0.2	0.2
J	-	-	-	0.0129	0.0129	0.00325

Consequently, we rewrite the expression

$$[\mathbf{Q}] = \sum_{l=0}^{\infty} \mathbf{N}_0^T [\mathbf{Z}^2]^l \mathbf{M}_0 / (N \lambda^{2l}). \quad (\text{B2})$$

Using the geometric sequence summation calculation, we get Eq. (24) in the main text

$$[\mathbf{Q}] = \frac{1}{N} \mathbf{N}_0^T \left(\mathbf{1} - \frac{[\mathbf{Z}^2]}{\lambda^2} \right)^{-1} \mathbf{M}_0. \quad (\text{B3})$$

The matrix $[\mathbf{Z}^2]$ can be decomposed as $\mathbf{D} + \mathbf{O}$, where $\mathbf{D} \in \mathbb{R}^{N \times N}$ is a diagonal matrix, and $\mathbf{O} \in \mathbb{R}^{N \times N}$ is a matrix of identical elements with block structure. The entries in matrix \mathbf{D} are determined by both the reciprocal and chain strengths, and the entries in matrix \mathbf{O} are determined by the chain motif strength. Furthermore, the matrix \mathbf{O} can be decomposed and expressed as

$$\mathbf{O} = \mathbf{U}_o \mathbf{V}_o^T; \quad \mathbf{U}_o, \mathbf{V}_o \in \mathbb{R}^{N \times R_o} \quad (\text{B4})$$

where the rank of \mathbf{O} is $R_o \ll P$. Then, we use the Woodbury matrix identity: given a square invertible $N \times N$ matrix $\mathbf{1} - \mathbf{D}/\lambda^2$, two $N \times R_o$ matrices \mathbf{U}_o and \mathbf{V}_o , \mathbf{A} and \mathbf{B} the invertible $N \times N$ matrices

$$\mathbf{A} = \left(\mathbf{1} - \frac{\mathbf{D}}{\lambda^2} \right) = \text{diag} \left(\left\{ \frac{\lambda^2 - D_{ii}}{\lambda^2} \right\} \right) \quad (\text{B5})$$

$$\mathbf{B} = \left(\mathbf{1} - \frac{[\mathbf{Z}^2]}{\lambda^2} \right) = \left(\left(\mathbf{1} - \frac{\mathbf{D}}{\lambda^2} \right) - \frac{\mathbf{U}_o \mathbf{V}_o^T}{\lambda^2} \right) \quad (\text{B6})$$

we have

$$\mathbf{B}^{-1} = \mathbf{A}^{-1} + \frac{1}{\lambda^2} \mathbf{A}^{-1} \mathbf{U}_o \left(\mathbf{1}_{R_o} - \frac{1}{\lambda^2} \mathbf{V}_o^T \mathbf{A}^{-1} \mathbf{U}_o \right)^{-1} \mathbf{V}_o^T \mathbf{A}^{-1}. \quad (\text{B7})$$

Now, rather than computing the inverse of an $N \times N$ matrix $(\mathbf{1} - \mathbf{Z}/\lambda)$ (Eq. (21)), we calculate the inverse of a diagonal matrix \mathbf{A} and an $R_o \times R_o$ matrix $(\mathbf{1}_{R_o} - \mathbf{V}_o^T \mathbf{A}^{-1} \mathbf{U}_o/\lambda^2)$.

We substitute Eq. (B7) into Eq. (24), and then search for the solutions of the characteristic polynomial $f_Q(\lambda) = 0$ (Eq. (23)) to obtain the eigenvalue outliers λ_r , $r = 1 \dots R$.

2. Gaussian networks with uniform variance and correlations

In this section, we calculate the eigenvalue outliers in Gaussian networks with homogeneous chain motif strength (Sec. III B). We consider a homogeneous variance parameter σ^2 (Eq. (31)) and correlation coefficient of chain motifs τ^c , and the elements of $[\mathbf{Z}^2]$ are given by

$$\left[\sum_{k=1}^N z_{ik} z_{kj} \right] = \begin{cases} \sum_{q=1}^P \alpha_q \sigma^2 \tau^c, & i \neq j, \\ 0, & i = j. \end{cases} \quad (\text{B8})$$

In Eq. (26) we then have

$$\mathbf{D} = -\tau^c \sigma^2 \mathbf{1} \quad (\text{B9})$$

$$\mathbf{O} = \tau^c \sigma^2 \mathbf{e} \mathbf{e}^T \quad (\text{B10})$$

where $R_o = 1$ with $\mathbf{U}_o = \mathbf{e}$, $\mathbf{V}_o = \tau^c \sigma^2 \mathbf{e}$, and \mathbf{e} is an all-one vector. Substituting Eq. (B9) into Eq. (B7), we obtain

$$\mathbf{B}^{-1} = \frac{\lambda^2}{\lambda^2 + \tau^c \sigma^2} \mathbf{1} + \frac{\lambda^2 \tau^c \sigma^2}{(\lambda^2 - (N-1)\tau^c \sigma^2)(\lambda^2 + \tau^c \sigma^2)} \mathbf{e} \mathbf{e}^T. \quad (\text{B11})$$

Combining the rank-one mean connectivity structures as described in Eq. (29) and inserting this \mathbf{B}^{-1} (from Eq. (B11)) into Eq. (24) and subsequently into Eq. (23)

$$\begin{aligned} \lambda &= \frac{1}{N} \mathbf{n}_0^T \mathbf{B}^{-1} \mathbf{m}_0 \\ \mathbf{m}_0 &= [1 \dots]^T = \mathbf{e} \\ \mathbf{n}_0 &= [N J^0 \dots, -N g J^0 \dots]^T \end{aligned} \quad (\text{B12})$$

we obtain the polynomial equation for λ :

$$\lambda = \frac{\lambda^2 \lambda_0}{\lambda^2 + \tau^c \sigma^2} + \frac{N \lambda^2 \tau^c \sigma^2 \lambda_0}{(\lambda^2 + \tau^c \sigma^2)(\lambda^2 - (N-1)\tau^c \sigma^2)}. \quad (\text{B13})$$

It's important to note that we focus on the case where λ is an outlier, indicating $\lambda^2 > \sigma^2$. Additionally, the correlation coefficient τ^c falls within the range $[-1, 1]$, ensuring that λ satisfies $\lambda \neq 0$ and $\lambda^2 + \tau^c \sigma^2 > 0 \neq 0$. These conditions lead us to the polynomial equation expressed in Eq. (32) in the main text

$$\lambda = \frac{\lambda_0 \mp \sqrt{\lambda_0^2 + 4(N-1)\tau^c \sigma^2}}{2}. \quad (\text{B14})$$

Analogously, in Gaussian networks with homogeneous reciprocal motif strength, the elements of $[\mathbf{Z}^2]$ are given by

$$\left[\sum_{k=1}^N z_{ik} z_{kj} \right] = \begin{cases} 0, & i \neq j, \\ \sum_{q=1}^P \alpha_q \sigma^2 \tau^r, & i = j. \end{cases} \quad (\text{B15})$$

There is only the diagonal matrix \mathbf{D} which has identical non-zero diagonal entries $\tau^r \sigma^2$, therefore

$$\mathbf{B}^{-1} = \mathbf{A}^{-1} = \frac{\lambda^2}{\lambda^2 - \tau^r \sigma^2} \mathbf{1}. \quad (\text{B16})$$

Thus the polynomial equation for determining the eigenvalues of \mathbf{J} with solely reciprocal motifs is

$$\lambda = \frac{\lambda_0 \lambda}{\lambda^2 - \tau^r \sigma^2}. \quad (\text{B17})$$

Given that $\lambda \neq 0$, we have

$$\lambda^2 - \lambda \lambda_0 - \tau^r \sigma^2 = 0, \quad (\text{B18})$$

which leads to the Eq. (36) in the main text and gives

$$\lambda = \frac{\lambda_0 \mp \sqrt{\lambda_0^2 + 4\tau^r \sigma^2}}{2}. \quad (\text{B19})$$

3. Gaussian networks with heterogeneous variance and correlations

Next, we derive the eigenvalues of a connectivity matrix with heterogeneous variance and correlations. Rather than considering the general case where the variance of synaptic weights is determined by the populations of both pre- and postsynaptic neurons, we assume here that it depends solely on the population of the presynaptic neuron. Consequently, we define the variance as $\sigma_{pq}^2 = \sigma_q^2/N$. For the correlation coefficients for chain motifs, we assume that they depend on the populations of the presynaptic neurons of the two involved synapses, thereby introducing heterogeneity in τ_{pq}^c . Following these assumptions, the elements of $[\mathbf{Z}^2]$ are

$$\left[\sum_{k=1}^N z_{ik} z_{kj} \right] = \begin{cases} \sum_{q=1}^P \alpha_q \sigma_q \sigma_s \tau_{qs}^c, & i \neq j, \\ 0, & i = j, \end{cases} \quad (\text{B20})$$

where the neuron with index i belongs to population p while the neuron with index j belongs to population s with $p, q, s \in \{E, I\}$. The matrix $[\mathbf{Z}^2]$ therefore has a columnar structure where all elements corresponding to $j \in E$ are identical, as are those for $j \in I$. Consequently, we express

$$\begin{aligned} [\mathbf{Z}^2]_{ij} &= \alpha_E \sigma_E^2 \tau_{EE}^c + \alpha_I \sigma_I \sigma_E \tau_{IE}^c = Z_E^2, j \in E \\ [\mathbf{Z}^2]_{ij} &= \alpha_E \sigma_E \sigma_I \tau_{EI}^c + \alpha_I \sigma_I^2 \tau_{II}^c = Z_I^2, j \in I \end{aligned} \quad (\text{B21})$$

Analogously to the homogeneous case, the matrix $[\mathbf{Z}^2]$ can be decomposed into a diagonal matrix \mathbf{D} and a block-like matrix \mathbf{O} . Since the impact of \mathbf{D} on the eigenvalues is

negligible compared to that of \mathbf{O} , for ease of mathematical analysis, we ignore \mathbf{D} and focus only on the block-like matrix \mathbf{O} . Moreover, as per Eq. (B21), the matrix \mathbf{O} has a unit rank structure, expressed as

$$\begin{aligned} \mathbf{O} &= \mathbf{U}_o \mathbf{V}_o^\top \\ \mathbf{U}_o &= \mathbf{e} \\ \mathbf{V}_o &= [Z_E^2 \dots, Z_I^2 \dots]^\top. \end{aligned} \quad (\text{B22})$$

By substituting Eq. (B22), we have

$$\begin{aligned} \mathbf{A} &= \mathbf{1} \\ \mathbf{B} &= (\mathbf{1} - \frac{1}{\lambda^2} \mathbf{U}_o \mathbf{V}_o^\top) \end{aligned} \quad (\text{B23})$$

therefore

$$\mathbf{B}^{-1} = \mathbf{1} + \frac{1}{\lambda^2 - (N_E Z_E^2 + N_I Z_I^2)} \mathbf{U}_o \mathbf{V}_o^\top. \quad (\text{B24})$$

By integrating the rank-one mean structure from Eq.(29) with the inverse matrix described in Eq.(B24) into Eq. (24), we obtain the polynomial equation

$$\lambda = \lambda_0 + \frac{\lambda_0 (N_E Z_E^2 + N_I Z_I^2)}{\lambda^2 - (N_E Z_E^2 + N_I Z_I^2)}. \quad (\text{B25})$$

The non-zero solutions can be expressed as

$$\lambda = \frac{\lambda_0 \mp \sqrt{\lambda_0^2 + 4(N_E Z_E^2 + N_I Z_I^2)}}{2} \quad (\text{B26})$$

Similarly, in Gaussian networks characterized by heterogeneous reciprocal motif strengths, the elements of $[\mathbf{Z}^2]$ are

$$\left[\sum_{k=1}^N z_{ik} z_{kj} \right] = \begin{cases} 0, & i \neq j, \\ \sum_{q=1}^P \alpha_q \sigma_q \sigma_p \tau_{pq}^r, & i = j. \end{cases} \quad (\text{B27})$$

where the neuron with index i belongs to population p . In the simplified two-population scenario, the matrix $[\mathbf{Z}^2]$ only has non-zero diagonal elements. All diagonal elements corresponding to $i \in E$ are identical, as are those for $i \in I$. We denote these two values as

$$\begin{aligned} [\mathbf{Z}^2]_{ii} &= \alpha_E \sigma_E^2 \tau_{EE}^r + \alpha_I \sigma_I \sigma_E \tau_{IE}^r = Z_E^2, i \in E \\ [\mathbf{Z}^2]_{ii} &= \alpha_E \sigma_E \sigma_I \tau_{EI}^r + \alpha_I \sigma_I^2 \tau_{II}^r = Z_I^2, i \in I. \end{aligned} \quad (\text{B28})$$

The inverse matrix $\mathbf{A}^{-1} = \text{diag}(\{\lambda^2/(\lambda^2 - D_{ii})\})$ is therefore a diagonal matrix

$$\begin{bmatrix} \frac{\lambda^2}{\lambda^2 - Z_E^2} & & & & \\ & \ddots & & & \\ & & \ddots & & \\ & & & \ddots & \\ & & & & \frac{\lambda^2}{\lambda^2 - Z_I^2} \end{bmatrix}$$

which, combined with the mean unit rank structure, leads to the polynomial equation for the eigenvalues as

$$\lambda = \frac{N_E J^0 \lambda^2}{\lambda^2 - Z_E^2} - \frac{N_I g J^0 \lambda^2}{\lambda^2 - Z_I^2}. \quad (\text{B29})$$

By replacing Z_E^2 , Z_I^2 with Eq. (B28) and solving this polynomial equation, we can theoretically obtain the eigenvalues of \mathbf{J} with heterogeneous reciprocal correlations [33].

Appendix C: Network constructions

1. Fully-connected Gaussian networks

To generate fully-connected networks with correlated Gaussian weights, we follow the standard procedure for

generating correlated Gaussian variables by forming linear combinations of uncorrelated variables [30].

For homogeneous networks we use

$$J_{ij} = J_{pq}^0 + \frac{\sigma}{\sqrt{N}} \left(\underbrace{\overbrace{sgn(\tau^c) \sqrt{|\tau^c|} \eta_i}^{\text{convergent}} + \overbrace{\sqrt{|\tau^c|} \eta_j - sgn(\tau^c) \sqrt{|\tau^c|} \mu_{ij} + \sqrt{|\tau^c|} \mu_{ji}}^{\text{divergent}}}_{\text{chain}} + \underbrace{sgn(\tau^r) \sqrt{|\tau^r/2|} \nu_{ij} + \sqrt{|\tau^r/2|} \nu_{ji}}_{\text{reciprocal}} + \underbrace{\sqrt{1 - 4|\tau^c| - |\tau^r|} y_{ij}}_{\text{independent}} \right) \quad (\text{C1})$$

where the post- and presynaptic neurons i and j belong to population p and q , τ^c denotes the homogeneous chain type correlations between connections in a chain circuit crossing neuron i or j , τ^r represents the homogeneous reciprocal type correlation between connections J_{ij} and J_{ji} , and $\eta_i, \mu_{ij}, \nu_{ij}$, and y_{ij} are i.i.d. normal random variables.

Note that, following [30, 32], we generate chain motifs by simultaneously creating divergent and convergent motifs (Appendix A) through the shared random variable η , so that $|\tau^{div}| = |\tau^{con}| = |\tau^c|$. This is not the most general approach, as we could further add two independent random variables, α_i and β_i , for synaptic couplings that

start or end at neuron i , respectively. These random variables would independently contribute to τ^{div} and τ^{con} , but not to τ^c or τ^r . However, since only chain and reciprocal motifs influence $[\mathbf{Z}^2]$ and the eigenvalues of the dynamics, we focus here on a simplified scenario where the divergent and convergent correlations fully characterize the chain motifs.

The terms $-sgn(\tau^c) \sqrt{|\tau^c|} \mu_{ij} + \sqrt{|\tau^c|} \mu_{ji}$ eliminate the diagonal reciprocity introduced by convergent and divergent motifs, the coefficient of the independent variable y_{ij} imposes the constraint that $1 - 4|\tau^c| - |\tau^r| > 0$.

For networks with population-dependent variances and correlations, we use

$$J_{ij} = J_{pq}^0 + \sigma_{pq} \left(sgn(\tau_{pq}^c) \sqrt{|\tau_{pq}^c|} \eta_i^{(q)} + \sum_{x=1}^P \sqrt{|\tau_{qx}^c|} \eta_j^{(x)} - sgn(\tau_{pq}^c) \sqrt{|\tau_{pq}^c|} \mu_{ij}^{(q)} + \sqrt{|\tau_{qp}^c|} \mu_{ji}^{(p)} + sgn(\tau_{pq}^r) \sqrt{|\tau_{pq}^r/2|} \nu_{ij} + \sqrt{|\tau_{pq}^r/2|} \nu_{ji} + c_{rm,pq} y_{ij} \right) \quad (\text{C2})$$

$$c_{rm,pq} = \sqrt{1 - 2|\tau_{pq}^c| - |\tau_{qp}^c| - \sum_{x=1}^P |\tau_{qx}^c| - |\tau_{pq}^r|}$$

where the pre-synaptic neuron with index j belongs to population q , and the post-synaptic neuron with index i belongs to population p . Here, τ_{pq}^c and τ_{pq}^r denote the population-dependent chain and reciprocal correlation coefficients, while $c_{rm,pq}$ is a coefficient setting the magnitude of the independent part of the synaptic variance. The entries in vectors $\boldsymbol{\eta}^{(p)} \in \mathbb{R}^N$, $p = 1 \dots P$, ma-

trices $\mathbf{U}^{(p)}$, $p = 1 \dots P$, \mathbf{V} and $\mathbf{Y} \in \mathbb{R}^{N \times N}$ are i.i.d. random variables following the normal distribution $\mathcal{N}(0, 1)$.

2. Sparse networks

We use the SONENT algorithm [34] to generate sparse networks with predefined local motifs. In brief, the occurrence probabilities of different motifs (Eq. (38)) are determined by the in-degree, out-degree, and full, joint-degree distributions of the units within the sparse networks. For each neuron in the network, SONENT samples pairs of in- and out-degree values from the full-degree distribution $p_d(x, y)$, and then assigns a non-zero connection from neuron j to i with a probability proportional to $x_i y_j$, where the proportionality constant sets the sparsity in the network.

More specifically, the in-degree distribution $p_{in}(x)$ is associated with the convergent motifs probability ρ^{con} , the out-degree distribution $p_{out}(y)$ is associated with the divergent motifs probability ρ^{div} , the full-degree distribution $p_d(x, y)$ is associated with the chain motifs probability ρ^c , and $p_{common}(x, y)$ is associated with the reciprocal motifs probability ρ^r . These relationships are expressed as

$$\begin{aligned}
 \langle x^2 \rangle &= \int x^2 p_{in}(x) dx = \rho^{con} N^2 \\
 \langle y^2 \rangle &= \int y^2 p_{out}(y) dy = \rho^{div} N^2 \\
 \langle xy \rangle &= \int xy p_d(x, y) dx dy = \rho^c N^2 \\
 \langle \nu \rangle &= \int \nu p_{common}(x, y) d\nu = \rho^r N.
 \end{aligned} \tag{C3}$$

Here ν represents the number of common nodes in x and y . Therefore, once we define the motif probabilities, we can derive the degree distributions based on the method-

ology outlined in [34, 70].

As for fully-connected Gaussian networks, for simplicity, we assume $\rho^{con} = \rho^{div} = \rho^c$, therefore $\{x_i = y_i\}_{i=1\dots N}$ and $p_d(x, y)$ has a Gaussian copula with correlation coefficient 1.

Practically, implementing SONENTs requires defining three types of parameters [34]. First, the marginal probability of synaptic couplings, denoted by p . Second, the probabilities of the reciprocal, convergent, divergent, and chain motifs deviating from independence, denoted by α_{recip} , α_{conv} , α_{div} , α_{chain} , respectively. Lastly, the correlation coefficient of the Gaussian copula. All these parameters can be analytically mapped to the parameters we used here to characterize the sparse network with chain motifs:

SONETs	Our Parameters	
$p =$	c	
$p^2(1 + \alpha_{recip}) =$	ρ^r	(C4)
$p^2(1 + \alpha_{conv}) =$	ρ^c	
$p^2(1 + \alpha_{div}) =$	ρ^c	
$p^2(1 + \alpha_{chain}) =$	ρ^c	

The second and third lines for the convergent and divergent motif statistics are derived by considering the relationship between chains and convergent/divergent motifs (see Appendix. A), that is, the correlation coefficient of the Gaussian copula is 1.

Appendix D: Supplementary figures.

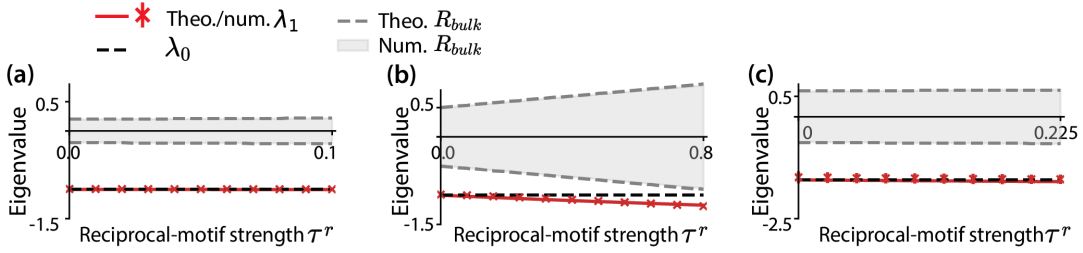


FIG. D.1. Eigenvalues of networks featuring reciprocal motifs. In subplots (a,b), results are presented for networks with Gaussian-distributed synaptic couplings. Subplots (a) and (b) show how the unique eigenvalue outlier λ_1 and the radius of the eigenvalue bulk R_{bulk} change as the statistics of the reciprocal motifs τ^r increase. The red error bars with asterisks represent the numerically obtained λ_1 from 30 network realizations, the red lines represent the theoretical predictions obtained using Eqs.(34) and (36). Gray areas illustrate the area of eigenvalue bulks obtained numerically, with gray dash-lines representing the theoretical predictions [30]. The black dash-lines indicate the unperturbed eigenvalue λ_0 of the mean connectivity. In subplot (a), the network parameters are the same as those used in Fig 2: $\sigma = 0.2$ and τ^r ranges from 0 to 0.1. In subplot (b), the networks have parameters $\sigma = 0.5$, and τ^r ranges from 0 to 0.8. Subplots (c) exhibit results for sparse networks. Figure descriptions are consistent with those in subplots (a,b).

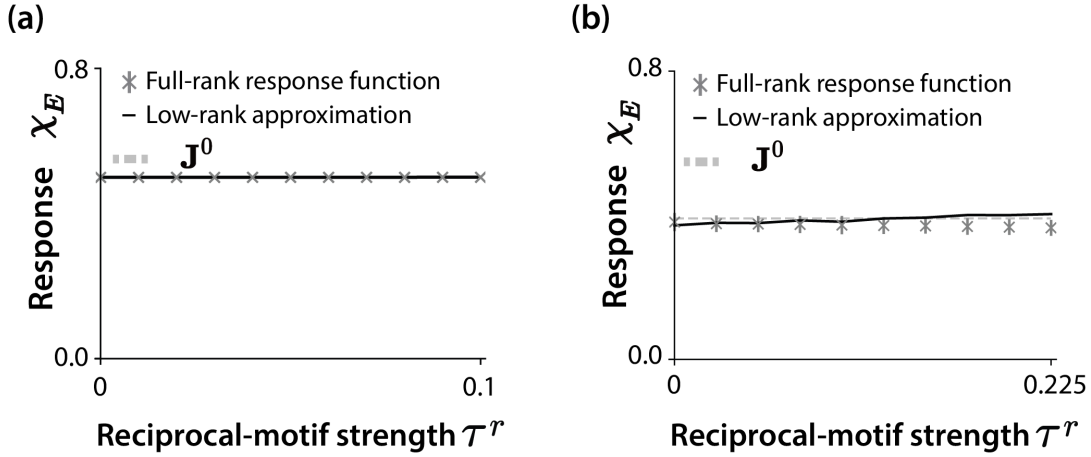


FIG. D.2. Mean response χ_E of the excitatory neuron population in response to the time-invariant uniform input I^{ext} in networks with only reciprocal motifs. Subplots (a) corresponds to Gaussian networks, while subplots (b) corresponds to sparse networks. Network parameters remain consistent with those provided in Figs 6 and 9.

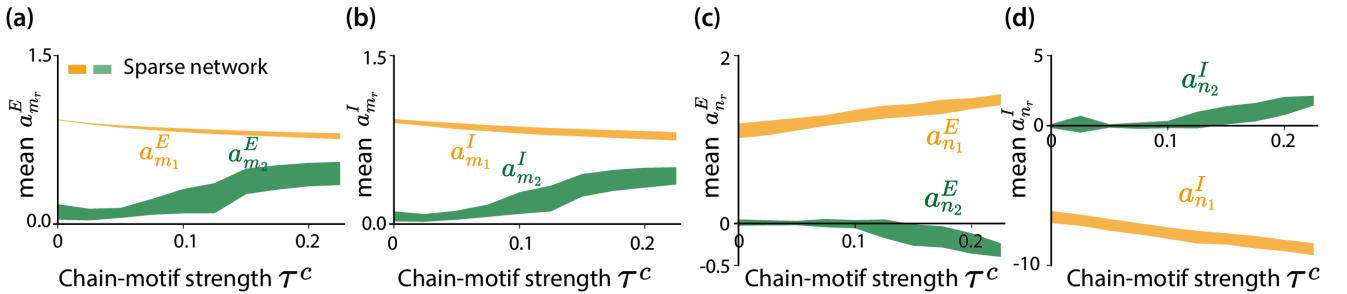


FIG. D.3. Population-averaged mean of entries on connectivity vectors for sparse networks featuring chain motifs. Figure descriptions are identical to those in Fig. 8, except that the network parameters are consistent with those used in Fig. 10 (see TABLE II).

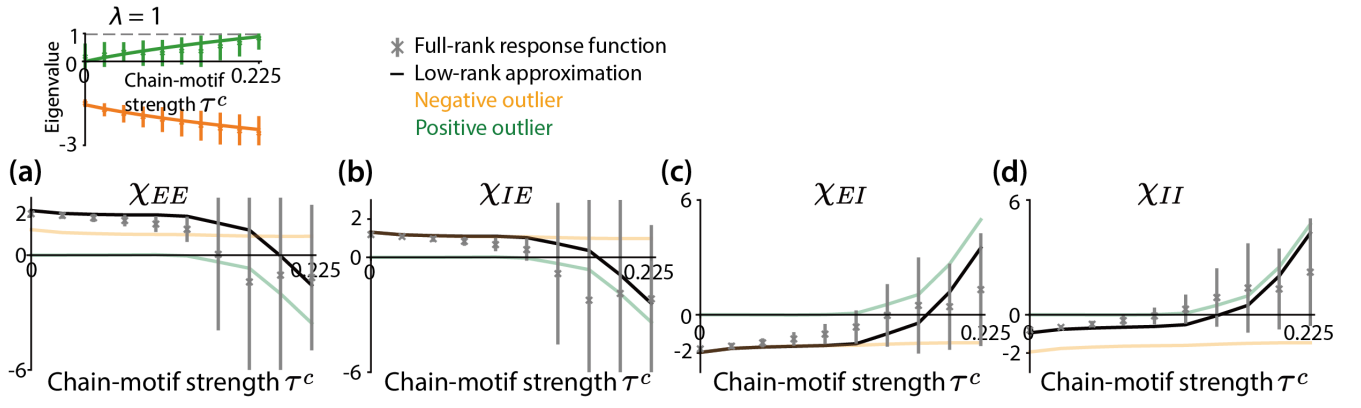


FIG. D.4. Impact of chain motifs on the mean response χ_{pq} of population p to uniform inputs to population q , in sparse excitatory-inhibitory networks. Figure descriptions are identical to those in Fig. 10, except that the network parameters are consistent with those used in Figs 8, 9 (see TABLE II).